Determining Cosmological Parameters from the Brightest SDSS Quasars

A Thesis Submitted to the
College of Graduate Studies and Research
in Partial Fulfillment of the Requirements
for the degree of Master of Science
in the Department of Physics and Engineering Physics
University of Saskatchewan
Saskatoon

By
Daryl Janzen

Permission to Use

In presenting this thesis in partial fulfilment of the requirements for a Postgraduate degree from the University of Saskatchewan, I agree that the Libraries of this University may make it freely available for inspection. I further agree that permission for copying of this thesis in any manner, in whole or in part, for scholarly purposes may be granted by the professor or professors who supervised my thesis work or, in their absence, by the Head of the Department or the Dean of the College in which my thesis work was done. It is understood that any copying or publication or use of this thesis or parts thereof for financial gain shall not be allowed without my written permission. It is also understood that due recognition shall be given to me and to the University of Saskatchewan in any scholarly use which may be made of any material in my thesis.

Requests for permission to copy or to make other use of material in this thesis in whole or part should be addressed to:

Head of the Department of Physics and Engineering Physics
116 Science Place
University of Saskatchewan
Saskatoon, Saskatchewan
Canada
S7N 5E2

Abstract

According to current cosmological theory, the rate of expansion of the universe depends on the average energy densities of matter, radiation, and a possible vacuum energy described by a cosmological constant, Λ, in the Einstein equation. Observations of galaxies and radiation, along with an assumption that we hold no special place in the universe, imply an isotropic and homogeneous energy distribution, for which the universal rate of expansion for most of the history of the universe may be constructed to depend only on present values of the dimensionless matter and vacuum energy density parameters, Ω_M and Ω_Λ, respectively, and the present rate of expansion of the universe, H_0. Over the past decade, much progress has been made in determining the values of the three density parameters using a variety of independent methods. In particular, observations of type Ia supernovae in the late 1990s provided the first evidence that $\Lambda \neq 0$ and that universal expansion is accelerating. This study has determined values for Ω_M and Ω_Λ using the brightest quasars in the Sloan Digital Sky Survey Data Release 5, which are located at a range of distances – equivalently, a range of lookback times – that have not been accessible through any other observations. After fitting the apparent magnitudes of the brightest quasars at various redshifts to the distance modulus equation with a luminosity evolution term, values for the density parameters were determined to be $\Omega_M = 0.07$ and $\Omega_\Lambda = 1.13$.

Acknowledgements

Thanks to Professor Rainer Dick for your guidance in the development of this project. Your undying patience as I fussed over *all* of the little things was greatly appreciated.

Thanks to my family, Kim and Amalia, for giving me hope at times when I had none, for providing wonderful perspective when this project wasn't cooperating, and for celebrating with me when it was.

For my parents,

who have always done everything in their power to support me.

Contents

List of Tables

List of Figures

List of Abbreviations

AGN	Active galactic nucleus/nuclei
CBR	Cosmic background radiation
CDF	Cumulative distribution function
CDM	Cold dark matter
CMB	Cosmic microwave background (the current CBR)
FRW	Friedmann-Robertson-Walker; as in FRW cosmological models
GEVD	Generalized extreme value distribution
PDF	Probability density function
SCP	Supernova Cosmology Project
SDSS (DR5)	Sloan Digital Sky Survey (Data Release 5)
SN(e) Ia	Type Ia Supernova(e)
QSO	Quasi-stellar object
WMAP	Wilkinson Microwave Anisotropy Probe

Chapter 1

Introduction

One of the main objectives in astronomy is to find new methods of determining the cosmological parameters which describe the expansion rate of our universe (see Figure 1.1). According to current cosmological theory, our universe can be described by a spacetime metric whose spatial component is multiplied by a time dependent *scale factor*. Furthermore, observations of distant galaxies over the past eighty years imply that the spatial component of the metric must be either a spherical, flat, or hyperbolic three-dimensional geometry. With these metrics, known as Robertson-Walker metrics, Einstein's field equation leads to a description of the large scale evolution of our universe which may depend on four independent parameters: the Hubble parameter, which describes the

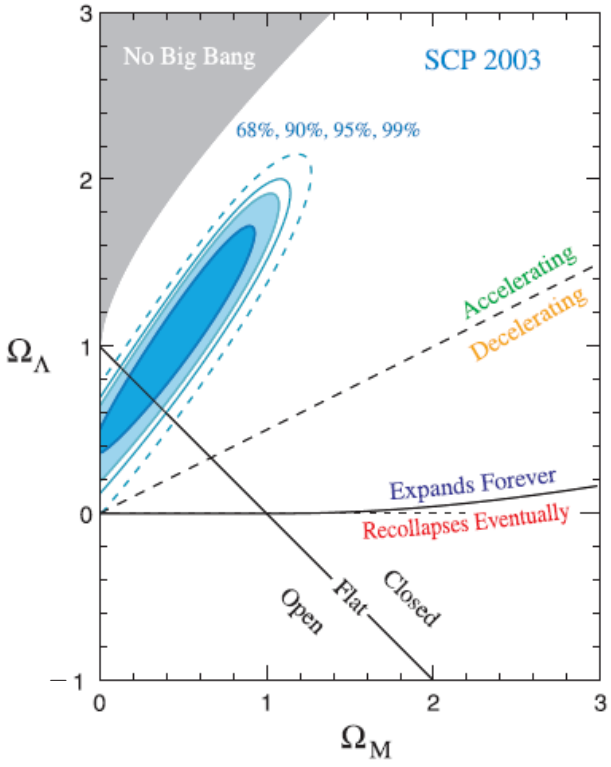

Figure 1.1: Different scenarios for the rate of expansion and final fate of the universe depending on Ω_M and Ω_Λ. The confidence regions shown in blue have been obtained by the Supernova Cosmology Project (Knop *et al.*, 2003).

expansion rate of the universe, and three cosmological density parameters, whose values depend upon the energy densities of matter, radiation, and a constant vacuum pressure, Λ. Determination of these parameters from various methods has given insight into the nature of the expansion of our universe. The universe is expanding at the present time, but there are many different possibilities for its future which depend on the values of the current matter and vacuum cosmological density parameters, Ω_M and Ω_Λ respectively, as displayed in Figure 1.1.

The most reliable observations available at present are consistent with an approximately flat universe ($\Omega_M + \Omega_\Lambda \approx 1$), which is accelerating in its expansion (Astier *et al.*, 2006; Riess *et al.*, 2007; Spergel *et al.*, 2003; Spergel *et al.*, 2007). The purpose of this thesis is to use existing data from quasar observations to develop a statistical method for determining the values of these two parameters. The quasars used in this analysis are located at distances which are not observable through any other observations, and should therefore provide new perspective to the theory of the universal expansion rate. The catalogue of quasars used in this analysis was compiled by Schneider *et al.* (2007) from the Sloan Digital Sky Survey (SDSS) Data Release 5 (DR5) and may be downloaded directly from the SDSS website (`www.sdss.org`).

Chapter 2

Friedmann-Robertson-Walker Cosmological Models

Currently, the best descriptions of our universe are thought to be given by Fiedmann-Robertson-Walker (FRW) cosmologies. In this Chapter, the basic premises of FRW models will be used to derive the equations that describe our universe which depend only on observable parameters.

2.1 Robertson-Walker Metrics

From observations of galaxies and the cosmic microwave background (CMB) we have seen that our universe appears isotropic on the largest scales, while maps of galaxies out to large distances have shown the universe to be nearly homogeneous with only a slight radial density gradient (Cole *et al.*, 2005; Colless *et al.*, 2001; Maddox *et al.*, 1990). For years, this radial density gradient was assumed to be negligible by proponents of the steady state cosmology so that the universe could be assumed to be homogeneous at all physical distances. Even with modern techniques, the radial density gradient, which has been observed by Cole *et al.* (2005) for galaxies in our near vicinity, may not be reliable due to effects of galaxy luminosity evolution and hierarchical merging history. However, given the expanding universe model of standard big bang cosmology, if the matter in the universe is actually homogeneously distributed we would expect to see this radial density gradient when observing increasingly distant objects because the finite speed of light implies that as we look deeper into space we are looking further back in time. Now, because the density gradient is uniform and isotropic, it is reasonable to make the assumption that the universe would appear this way from any galaxy, i.e. the universe is also homogeneous. This assumption is called Einstein's cosmological principle and it is a requirement of big bang cosmology (Peebles, 1993).

A homogeneous, isotropic, expanding cosmological geometry is described by *comoving* coordinates – time-independent coordinates multiplied by a time-dependent scaling. The simplest description of this type of geometry is given by the spatially flat Robertson-Walker metric,

$$ds^2 = -c^2dt^2 + a^2(t)\left[dr^2 + r^2(d\theta^2 + \sin^2\theta d\phi^2)\right], \tag{2.1}$$

where $a(t)$ is the scale factor. However, this metric only describes a spacetime geometry with

three-dimensional Euclidean space and is therefore only a special case of a homogeneous, isotropic cosmological spacetime geometry. In the mid 1930's, Robertson and Walker independently demonstrated that the full set of metrics which satisfy the cosmological principle can be written

$$ds^2 = -c^2dt^2 + a^2(t)\left[\frac{dr^2}{1-kr^2} + r^2(d\theta^2 + \sin^2\theta\ d\phi^2)\right] \tag{2.2}$$

(Robertson, 1935; Walker, 1935). Here, $k = 1, 0, -1$ correspond to spherical, flat, and hyperbolic spacetimes, respectively. The spherical metric is obtained from the analysis of the surface of the unit three-sphere and the hyperbolic metric is obtained by considering a Lorentz hyperboloid, which is the analog of the spherical geometry derived by embedding a three-surface in flat four-dimensional spacetime (Hartle, 2003). Traditionally, the spherical and hyperbolic spacetime geometries have been referred to as closed and open because of their asymptotic natures in a $\Lambda = 0$ universe (see Figure 1.1). However, in light of the strong evidence for a non-zero cosmological constant over the last decade (see, e.g., Knop *et al.*, 2003; Astier *et al.*, 2006; Riess *et al.*, 2007; Spergel *et al.*, 2007; Tonry *et al.*, 2003) these terms have lost their meaning and *should* be dropped.

2.2 Cosmological Redshift and Hubble's Constant

When Albert Einstein published his General Theory of Relativity (Einstein, 1915a,b,c), relating the geometry of spacetime to energy density, astronomers believed that our universe consisted only of the (static) Milky Way Galaxy. However, in 1917, Willem de Sitter made the first attempt at deriving a theoretical model for an evolving universe when he published a solution to Einstein's field equations which allowed for an expanding universe (de Sitter, 1917). Redshift observations of spiral nebulae conducted by Vesto M. Slipher at Lowell Observatory in the early part of the twentieth century supplied evidence that the universe was indeed expanding. Subsequently, Hubble (1926) offered conclusive evidence based on observations of Cepheid variable stars that the galaxy, Messier 33 – one of the few blueshifted spiral nebulae – was too far away to be a part of our Galaxy. By 1929, Hubble had determined distances to eighteen spiral nebulae through further Cepheid variable observations and with the use of Slipher's redshift measurements, came to an astonishing conclusion: there is a linear relationship between the redshift and distance of galaxies,

$$v = cz = H_0 d, \tag{2.3}$$

which is now known as Hubble's Law (Hubble, 1929). The Robertson-Walker metric can be used to determine the cosmological redshift, z, and Hubble's constant, H_0, in terms of a. Such relations may then be incorporated into the development of our cosmology so that we have a model based on observable physical parameters.

We begin this analysis by noting that the radial null curve of a photon directed toward us which

has been emitted by a nearby galaxy is given by

$$ds^2 = 0 = -c^2dt^2 + a^2(t)\frac{dr^2}{1-kr^2} \equiv -c^2dt^2 + a^2(t)d\chi^2. \tag{2.4}$$

Now if we consider a series of photons being emitted from this galaxy at a frequency $\omega_e = 2\pi/\delta t_e$ they will arrive here at a frequency $\omega_0 = 2\pi/\delta t_0$. If the series of photons began to leave the galaxy at time t_e and they first arrived here at t_0 we obtain

$$\chi = \int_{t_e}^{t_0} \frac{cdt}{a(t)} = \int_{t_e+\delta t_e}^{t_0+\delta t_0} \frac{cdt}{a(t)}. \tag{2.5}$$

For small δt_e and δt_0 the second integral differs from the first in that it will contain a small extension $c\delta t_0/a(t_0)$ in the upper limit and a small contraction $c\delta t_e/a(t_e)$ in the lower limit. These changes must equal one another to preserve equality of the two integrals. Thus, for the ratio of the frequency of an observed photon to the frequency at which it was emitted we obtain

$$\frac{\omega_0}{\omega_e} = \frac{a(t_e)}{a(t_0)}. \tag{2.6}$$

This relation can be used to determine the cosmological redshift

$$1 + z \equiv \frac{\lambda_0}{\lambda_e} = \frac{\omega_e}{\omega_0} = \frac{a(t_0)}{a(t_e)}. \tag{2.7}$$

Now consider a photon emitted from a galaxy a short distance

$$d = a(t_0)\chi \tag{2.8}$$

away from us, so that χ is small at the time of reception. The time it takes the photon to reach us can be found from

$$(c\Delta t)^2 = a^2(t_0)\chi^2 + \mathcal{O}(\chi^3) \approx d^2. \tag{2.9}$$

Therefore, $t_e = t_0 - d/c$ and we can evaluate

$$cz \equiv \frac{\Delta\lambda}{\lambda} = \left[\frac{\dot{a}(t_0)}{a(t_0)}\right] d \qquad (d \text{ small}). \tag{2.10}$$

Comparing this result with (2.3), we find the connection between Hubble's constant and the geometry of spacetime:

$$H_0 \equiv \frac{\dot{a}(t_0)}{a(t_0)}. \tag{2.11}$$

Current data suggest that the value of Hubble's constant is somewhere near 73 (km/s)/Mpc (Spergel *et al.*, 2007). This value will be used for illustrative purposes in some future calculations.

Although H_0 has been measured by many different observations, its value is still not known with great precision; therefore, cosmologists prefer to write equations in terms of the Hubble parameter

$$h \equiv \frac{H_0}{100(\text{km/s})/\text{Mpc}}. \tag{2.12}$$

Although H_0 is no longer determined by plotting redshifts of galaxies against their distances, it is still quoted for historical reasons with units of (km/s)/Mpc. By including the conversion from kilometers to megaparsecs, it is clear that Hubble's constant actually has the dimensions of an inverse time. The inverse of H_0, known as the *Hubble time*, is a useful result in that it gives the age of the universe if it were to have a constant rate of expansion:

$$t_H = \frac{1}{H_0} = 9.78h^{-1} \text{ Gyr}. \tag{2.13}$$

Thus, for $h = 0.73$ we have the result $t_H = 13.4$ Gyr.

We will see later on that FRW cosmologies do not allow for a constant rate of spatial expansion as Hubble initially determined through observations of relatively close galaxies. This is due to the variability in time dependence of the energy densities of the various components of our universe, which we will see in §2.4. Hubble's constant is therefore only the current expansion rate of the universe; however, we will see in §2.5 that we can parameterize the equations used to describe the geometry of our universe so that Hubble's constant remains a very meaningful parameter.

2.3 The Friedmann and Acceleration Equations

At this point, we would like to derive an equation for the scale factor, $a(t)$, in the Robertson-Walker metric. This may be accomplished with the use of general relativity if we know something about the stress-energy of the universe. However, even before we begin to make any hypotheses about the energy content of the universe, we may derive two independent equations relating $a(t)$ to general terms for the pressure and energy density of the universe by inserting the Robertson-Walker metric into the Einstein equation of general relativity,

$$R_{\mu\nu} - \frac{1}{2}g_{\mu\nu}R = \kappa\left(T_{\mu\nu} - \Lambda g_{\mu\nu}\right). \tag{2.14}$$

Here, $R_{\mu\nu}$ and R are the Ricci tensor and Ricci scalar, respectively, $g_{\mu\nu}$ is the spacetime metric, $T_{\mu\nu}$ is the stress-energy tensor, Λ is a (possibly non-zero) constant, known as the cosmological constant, and the proportionality constant

$$\kappa = \frac{8\pi G}{c^4} = \frac{\hbar}{m_{Pl}^2 c^3} = 2.076 \times 10^{-43} \text{ N}^{-1}, \tag{2.15}$$

is determined by the Newtonian limit of the Einstein equation. Thus (2.14) describes gravity as a curvature of spacetime due to the energy and momentum it contains, where spacetime curvature enters into the Einstein equation through the Einstein tensor,

$$G_{\mu\nu} \equiv R_{\mu\nu} - \frac{1}{2}g_{\mu\nu}R, \tag{2.16}$$

where the definition of the Ricci tensor comes from the Riemann tensor; i.e.

$$R_{\mu\nu} = R^{\rho}{}_{\mu\rho\nu} = \partial_\rho \Gamma^{\rho}{}_{\mu\nu} - \partial_\nu \Gamma^{\rho}{}_{\mu\rho} + \Gamma^{\rho}{}_{\lambda\rho}\Gamma^{\lambda}{}_{\mu\nu} - \Gamma^{\rho}{}_{\lambda\nu}\Gamma^{\lambda}{}_{\mu\rho}, \tag{2.17}$$

and the Ricci scalar is the trace of the Ricci tensor,

$$R = R^{\mu}_{\ \mu} = g^{\mu\nu} R_{\mu\nu}. \tag{2.18}$$

The Christoffel symbols, $\Gamma^{\lambda}_{\ \mu\nu}$, are defined by

$$\Gamma^{\lambda}_{\ \mu\nu} = \frac{1}{2} g^{\lambda\rho} \left(\partial_\nu g_{\rho\mu} + \partial_\mu g_{\rho\nu} - \partial_\rho g_{\mu\nu} \right), \tag{2.19}$$

where $\partial_\alpha \equiv \partial / \partial x^\alpha$ and summation over repeated up-down indices is implied.

The Einstein tensor is the unique combination of curvature tensors which is linear in second order derivatives of the metric and satisfies

$$\nabla_\mu G^{\mu\nu} = \partial_\mu G^{\mu\nu} + \Gamma^{\mu}_{\ \mu\rho} G^{\rho\nu} + \Gamma^{\nu}_{\ \mu\rho} G^{\mu\rho} \equiv 0, \tag{2.20}$$

which is required by local conservation of energy-momentum,

$$\nabla_\mu T^{\mu\nu} = 0, \tag{2.21}$$

so that no additional higher-order constraints are placed on the metric (Einstein, 1915a).

Note that $\nabla_\mu g^{\mu\nu} \equiv 0$, so that any constant multiple of the metric may be included in the Einstein equation. This is what initially led Einstein to include the cosmological constant in (2.14) in an attempt to account for a static universe. The subsequent discovery by Hubble that the universe is expanding led Einstein to state that the cosmological constant was his "greatest blunder." However, observations of type Ia supernovae (SNe Ia) in the late 1990s resurrected the use of Λ in cosmology, when it was discovered that the universe's expansion is actually accelerating.

Now, using the above equations from general relativity we may derive expressions for the time dependence of the scale factor. By inserting the Robertson-Walker metric (2.2) into the Einstein tensor, we have the result,

$$G_{00} = 3 \frac{\dot{a}^2 + k}{a^2}, \tag{2.22}$$

$$G_{0j} = G_{i0} = 0, \tag{2.23}$$

$$G_{ij} = -\left(2 \frac{\ddot{a}}{a} + \frac{\dot{a}^2 + k}{a^2} \right) g_{ij}, \tag{2.24}$$

where for simplicity the units in $(2.22) - (2.24)$ and the remainder of this section have been set so that $c = 1$.

The Einstein equation (2.14) therefore implies that the spatially averaged form of the stress-energy tensor of the universe has the form of a perfect fluid,

$$T_{00} = \rho(t), \tag{2.25}$$

$$T_{0j} = T_{j0} = 0, \tag{2.26}$$

$$T_{ij} = p(t) g_{ij}. \tag{2.27}$$

Thus, we obtain two equations for the time dependence of the scale factor, which depend on the energy density and pressure of the universe:

$$\frac{\dot{a}^2 + k}{a^2} = \frac{\kappa}{3}(\rho + \Lambda), \tag{2.28}$$

$$2\frac{\ddot{a}}{a} + \frac{\dot{a}^2 + k}{a^2} = \kappa(\Lambda - p). \tag{2.29}$$

The first of these equations is known as the Friedmann equation and the second is generally referred to as the acceleration equation. Models that use the Friedmann equation to determine the scale factor in the Robertson-Walker metric are known as Friedmann-Robertson-Walker (FRW) models (Hartle, 2003).

By requiring compatibility of (2.28) and (2.29), a third equation can be obtained, which is nicer to deal with than (2.29):

$$\dot{\rho} = -3(\rho + p)\frac{\dot{a}}{a} \Leftrightarrow d(\rho a^3) = -p d\left(a^3\right). \tag{2.30}$$

These equations leave us with three degrees of freedom – $a(t)$, $\rho(t)$, and $p(t)$ – for the large-scale evolution of the universe. Thus, to completely determine this system a third independent equation, an equation of state, must be used:

$$p = p(\rho). \tag{2.31}$$

2.4 Energy Density Dependence on the Scale Factor

Current FRW cosmologies assume that the cosmological fluid consists of three components – matter, radiation, and vacuum – which have had only negligible interactions since the very early universe. Thus, these three components can be analyzed separately to determine the evolution of the universe.

The matter contained in the universe can be well approximated by a pressureless gas; i.e. $p_M = 0$, which is denoted as *dust* in cosmology. Integration of (2.30) therefore yields the matter energy density of the universe:

$$\rho_M(t) = \rho_M(t_0)\left[\frac{a(t_0)}{a(t)}\right]^3 \equiv \rho_M(t_0)\left(\frac{a_0}{a}\right)^3, \tag{2.32}$$

where t_0 is the *present* time. Hereafter, the present and time dependent scale factors will be denoted $a(t_0) \equiv a_0$ and $a(t) \equiv a$, respectively.

For a gas of particles with temperature $T \gg \frac{mc^2}{k_B}$, the pressure is given by

$$p_R = \frac{1}{3}\rho_R. \tag{2.33}$$

Therefore, the radiation component to the energy density – which includes neutrinos, as well as photons – will have this type of pressure. Integration of (2.30) yields

$$\rho_R(t) = \rho_R(t_0)\left(\frac{a_0}{a}\right)^4. \tag{2.34}$$

In the very early universe, when a was very small, the radiation density must have been larger than the matter density. During this epoch the universe was *radiation dominated*. However, this did not last long and for most of its history the universe has been *matter dominated*.

Finally, we must consider the energy density of the vacuum. Recent observations indicate that this vacuum energy should be a positive constant in spacetime (Astier *et al.*, 2006; Riess *et al.*, 2007; Spergel *et al.*, 2007). Thus, the vacuum energy density may be denoted

$$\rho_\Lambda = \Lambda. \tag{2.35}$$

(c.f. (2.28): if the vacuum energy density were zero, the cosmological constant would not appear in this equation.) The vacuum energy equation of state

$$p_\Lambda = w\rho_\Lambda \tag{2.36}$$

must therefore be written with $w = -1$. If $\Lambda \neq 0$, the vacuum energy eventually dominates the matter and radiation densities and the universe becomes *vacuum dominated*.

In fact, if we substitute the literature values from Spergel *et al.* (2007) for the current matter and vacuum energy densities, $\rho_{M,0}/\rho_\Lambda \approx 0.24/0.76$, into (2.32), along with the condition $\rho_M(t) \leq \rho_\Lambda$, we find that the universe has been vacuum dominated since the scale factor was roughly 68% its current value, or since $z = 0.47$. If we incorrectly assume a constant rate of expansion for the universe, we can estimate the *lookback time* to an object located at such a redshift from

$$t_\gamma = \int_{t_e}^{t_0} dt = \int_{a_e}^{a_0} \frac{da}{\dot{a}} = \frac{z}{H_0(1+z)} \approx 4.3 \text{ Gyr}. \tag{2.37}$$

This calculation must be an underestimate because if the assumed values for matter and vacuum energy density are indeed correct the universe would have been accelerating in its expansion throughout the era of vacuum domination (see 2.46). Therefore, photons from an object at this redshift would have had to travel longer through space which was initially not expanding as rapidly to be redshifted to this value. Later on, we will see how to accurately calculate lookback times (§2.5) and distances (§3.2) using redshifts.

2.5 Parameters of a FRW Cosmological Model

An important result, known as the *critical energy density*, is obtained by evaluating the Friedmann equation with $k = 0$ at the present time. In doing so, we determine

$$\rho_c \equiv \frac{3}{\kappa c^2} H_0^2. \tag{2.38}$$

Here, the cosmological constant has been included in ρ_c as the vacuum density portion of the critical density so that ρ_c contains the total energy density required for spacetime to be flat in our present universe.

Upon substitution of (2.12) and (2.15), we find

$$\rho_c \equiv \frac{3c^2}{8\pi G} H_0^2 = 5.64 \times 10^{-18} h^2 \text{ J m}^{-3}, \tag{2.39}$$

which corresponds to a critical mass density of $1.88 \times 10^{-26} h^2$ kg m^{-3}.

Using ρ_c, we can define three new parameters; the cosmological density parameters. We will see that the three density parameters, along with Hubble's constant, can be used to determine the large scale structure and evolution of the universe. The cosmological density parameters are defined as the ratios of the current matter, radiation, and vacuum energy densities to the critical density:

$$\Omega_M \equiv \frac{\rho_M(t_0)}{\rho_c}, \qquad \Omega_R \equiv \frac{\rho_R(t_0)}{\rho_c}, \qquad \Omega_\Lambda \equiv \frac{\rho_\Lambda(t_0)}{\rho_c}. \tag{2.40}$$

With these definitions we can write the total energy density as a function of the scale factor, a

$$\rho(a) = \rho_c \left[\Omega_M \left(\frac{a_0}{a} \right)^3 + \Omega_R \left(\frac{a_0}{a} \right)^4 + \Omega_\Lambda \right]. \tag{2.41}$$

The Friedmann equation (2.28) then yields

$$\begin{aligned} \dot{a} &= a_0 H_0 \sqrt{\Omega_M \frac{a_0}{a} + \Omega_R \frac{a_0^2}{a^2} + \Omega_\Lambda \frac{a^2}{a_0^2} - \frac{k}{a_0^2 H_0^2}} \\ &= a_0 H_0 \sqrt{\Omega_M \left(\frac{a_0}{a} - 1 \right) + \Omega_R \left(\frac{a_0^2}{a^2} - 1 \right) + \Omega_\Lambda \left(\frac{a^2}{a_0^2} - 1 \right) + 1}, \end{aligned} \tag{2.42}$$

where in the second line the factor $\frac{kc^2}{a_0^2 H_0^2}$ has been replaced by the evaluation of (2.28) at the present time, i.e.

$$\frac{kc^2}{a_0^2 H_0^2} = \Omega_M + \Omega_R + \Omega_\Lambda - 1. \tag{2.43}$$

We see that (2.42) is solvable if we know the values of the four parameters H_0, Ω_M, Ω_R, and Ω_Λ. Therefore, a complete solution to a FRW cosmological model – which seems to provide a good description of our universe – can be obtained from the determination of the four FRW cosmological parameters.

Observations of SNe Ia indicate that the universe is at least very near to being flat, with $\Omega_M \approx 0.3$ and $\Omega_\Lambda \approx 0.7$ (Astier *et al.*, 2006; Knop *et al.*, 2003; Riess *et al.*, 2007; Tonry *et al.*, 2003). Observations of the cosmic microwave background (CMB) are strongly in favor of a flat cosmology with photon density $\Omega_\gamma = 4.6 \times 10^{-5}$ (Mather *et al.*, 1999; Spergel *et al.*, 2007). Measurements using the Wilkinson Microwave Anisotropy Probe (WMAP) have provided upper bounds for the sum of the masses, $\sum m_\nu < 0.7$ eV, and cosmological energy density of effectively stable neutrinos, $\Omega_\nu < 0.0072/h^2 \approx 0.01$ (Spergel *et al.*, 2007). However, the value of the upper bound on $\sum m_\nu$ has dropped three orders of magnitude in the past forty years and continues to drop at a consistent rate as measurement techniques improve (see Yao *et al.*, 2006). In light of this, we will neglect the neutrino's contribution to the radiation energy density in the rest of our analysis, adopting $\Omega_R = \Omega_\gamma = 4.6 \times 10^{-5}$. Thus, (2.34) and (2.32) imply that at $z = 5$ (roughly the current

observation limit for quasars), $\rho_R/\rho_M \approx 10^{-3}$ for $\Omega_M = 0.24$. Therefore, a good description of the universe can be derived by neglecting radiation density when compared to dust and vacuum densities. Figure 1.1 in Chapter 1 shows the possible fates of our universe for various values of Ω_M and Ω_Λ, as described by (2.42). The confidence regions for these values, determined from observations of SNe Ia by the Supernova Cosmology Project (SCP), are illustrated with the blue ellipses on the left side of Figure 1.1. The SCP data suggest that our universe is accelerating in its expansion. If this is true, the universe should continue to accelerate forever.

In §2.4 we calculated an underestimate for the lookback time to when the universe first became vacuum dominated. Now we are able to solve (2.42) with $h = 0.73$, $\Omega_M = 0.24$, $\Omega_\Lambda = 0.76$, and $\Omega_R = 4.6 \times 10^{-5}$ for $a/a_0 = 0.68$:

$$\begin{aligned} t_L(z = 0.47) &= t_0 - t(\rho_M = \rho_\Lambda) \\ &= \int_{0.754a_0}^{a_0} \frac{da}{a_0 H_0 \sqrt{\Omega_M \left(\frac{a_0}{a} - 1\right) + \Omega_R \left(\frac{a_0^2}{a^2} - 1\right) + \Omega_\Lambda \left(\frac{a^2}{a_0^2} - 1\right) + 1}} \\ &= 4.7 \text{ Gyr}. \end{aligned} \tag{2.44}$$

Now if we evaluate (2.32) and (2.34) with these same values for the density parameters, we find that $\rho_R \geq \rho_M$ when $z \approx 5000$, approximately 13.73 billion years ago. Evaluating $\lim_{a\to 0} t_L$, we find that this transition occurred a mere 28000 years after the big bang.

Another important result is the redshift at which the universe began accelerating, z_{accel}. This value may be estimated from (2.42) by setting $\ddot{a} = 0$ and neglecting the term containing Ω_R compared to the matter and vacuum density terms:

$$\begin{aligned} \ddot{a}_{accel} \equiv 0 &\approx \frac{a_0^2 H_0^2}{2} \left(-\frac{a_0}{a_{accel}^2} \Omega_M + 2 \frac{a_{accel}}{a_0^2} \Omega_\Lambda \right), \\ \Rightarrow \frac{a_{accel}}{a_0} &\approx \left(\frac{\Omega_M}{2\Omega_\Lambda} \right)^{1/3}. \end{aligned} \tag{2.45}$$

Using (2.10), we find the result,

$$z_{accel} = \frac{a_0}{a_{accel}} - 1 \approx 0.85. \tag{2.46}$$

Let us go a step further with this analysis so that we may fully appreciate the importance of determining these cosmological parameters to great precision. I have already mentioned the present cosmic background radiation (CBR), the CMB, which was left over as a result of the big bang. In the standard hot big bang model, this radiation is predicted as an explanation for observed energies and chemical abundances in the universe. To see what the CBR should look like, we start by noting that the mean number of photons per mode at temperature T is given by the Planck function

$$\langle N \rangle = \frac{1}{e^{hc/k_B T\lambda} - 1} \tag{2.47}$$

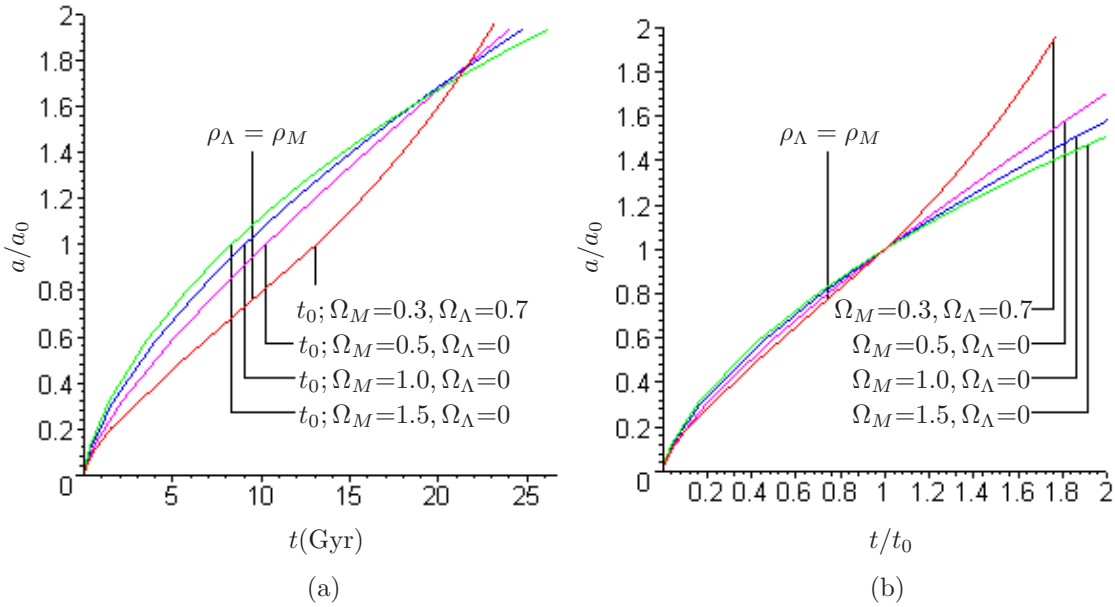

Figure 2.1: Evolution of the scale factor calculated from (2.42) for different values of the FRW cosmological parameters. All curves were calculated with $\Omega_R = 4.6 \times 10^{-5}$. In (a), the present age of the universe is indicated as a point on each curve. The values of t_0 for the spherical, flat, and hyperbolic $\Lambda = 0$ models, and the $\Lambda \neq 0$ model, are 8.30, 9.05, 10.23, and 13.09 Gyr, respectively. In (b), the time axis has been divided by the present age of the universe for each of the curves' respective value of t_0 so as to illustrate the possible history and evolutionary paths of $a(t)$ as seen from our perspective.

(Peebles, 1993). The hot big bang model predicts that shortly after the big bang the temperature of the CBR must have been high enough for the fusion of hydrogen into helium. During this time, radiation and matter would have been coupled in a plasma. Because the universe has always been expanding in the big bang model, there must have been a point in time when the temperature dropped below that needed to maintain the plasma. After this time, known as the decoupling era, these photons would have been released from matter, able to travel unimpeded for the rest of time. From (2.47) and (2.7) we find that after decoupling, while the mean number of photons per mode has remained constant the temperature has changed inversely proportional to the scale factor:

$$T \propto 1/a(t). \tag{2.48}$$

If we further assume that all anisotropies in the present universe are due to gravitational interactions, so that at the time of decoupling the CBR would have been in thermal equilibrium and hence, the same for all modes, we find that the temperature of the radiation is given by

$$T(t) = T_0 \frac{a_0}{a(t)} = T_0(1+z), \tag{2.49}$$

where T_0 is the temperature of the CMB.

Gamow (1948) and Alpher and Herman (1948) estimated that to account for the abundance of helium in the universe ($\sim$ 24% by mass) the present temperature of the CBR should be $\sim$ 5 K. The discovery of the 3.5 ± 1.0 K CMB by Penzias and Wilson (1965), who were working at the Bell Telephone Laboratories in Holmdel, New Jersey, was the observational evidence needed to bring wide acceptance to the big bang theory. Today, the CMB has a measured value of $T_0 = 2.275 \pm 0.001$ K (Mather *et al.*, 1999).

From the above example, we find that when ρ_M overcame ρ_R the temperature of the radiation was $\sim$ 1400 K. From the results of Peebles (1993), but with current observational values for T_0 and the baryon density $\Omega_B = 0.0224 \pm 0.0009$ we find that the redshift corresponding to decoupling is $z \approx 2000$. This redshift corresponds to roughly 150 000 years after the big bang.

Obviously it is of great interest to determine the values of the FRW cosmological parameters with great precision because they determine the ultimate fate of our universe; whether it will expand forever, or eventually recollapse in a *big crunch*. The evolution of the scale factor for different values of the cosmological parameters is illustrated in Figure 2.1. If the universe expands forever, all of the gas that is used as fuel for stars will eventually be exhausted and the universe will become dark. Dead stars and planets will lose energy and spiral into supermassive black holes in galactic cores. Eventually, all of the energy in these supermassive black holes will be lost through Hawking radiation and the universe will be completely barren. On the other hand, if the universe recollapses in a big crunch every form of matter we know of will cease to exist when the universe returns to a singularity. However, in this scenario there is a chance that a new big bang may happen.

Chapter 3

Determination of Cosmological Parameters from Observations of Quasars: Background Information and Theoretical Framework

In the previous section we derived the necessary theory to understand the evolutionary history and the geometry of the universe in a FRW cosmology. In the end, the theory contained four parameters which must be determined experimentally. In this chapter, we will see how apparent brightnesses of quasars can be linked to the FRW cosmological parameters, so that in Chapter 4 we may develop the analytical framework necessary to determine these parameters using a statistical approach. However, some background information is necessary before we may develop this model.

3.1 Quasars

Quasars are some of the most peculiar objects observable in the universe. They are small, starlike objects, with peculiar spectra, and traditionally have been observed very close to galaxies (Carroll and Ostlie, 2007). We know that quasars are small because observations of their luminosities have shown that they change in brightness over very short time scales. For an object to change in brightness over the course of a few years, as is the case with quasars, the maximum size of the object can be calculated by assuming the object uniformly changes its brightness in an instant. The maximum diameter of a quasar that changes from maximum to minimum brightness in an observed time, T is then cT. For quasars, this implies that their maximum diameters can only be about a few lightyears. Over the decades since their discovery many theories have been constructed which try to explain what a quasar is.

The name quasar has been derived from quasi-stellar object (QSO); the name originally given to these objects because they appear in the sky as stars, but their spectra are very different from stars. The first quasar discovery was made when Matthews and Sandage (1963) were searching for an optical counterpart to an observed radio source, 3C 48. At the centre of the radio source they observed a 16th magnitude starlike object with broad *emission* lines (stellar spectra generally contain absorption lines) and a redshift that was eventually measured to be $z = 0.367$ (Greenstein

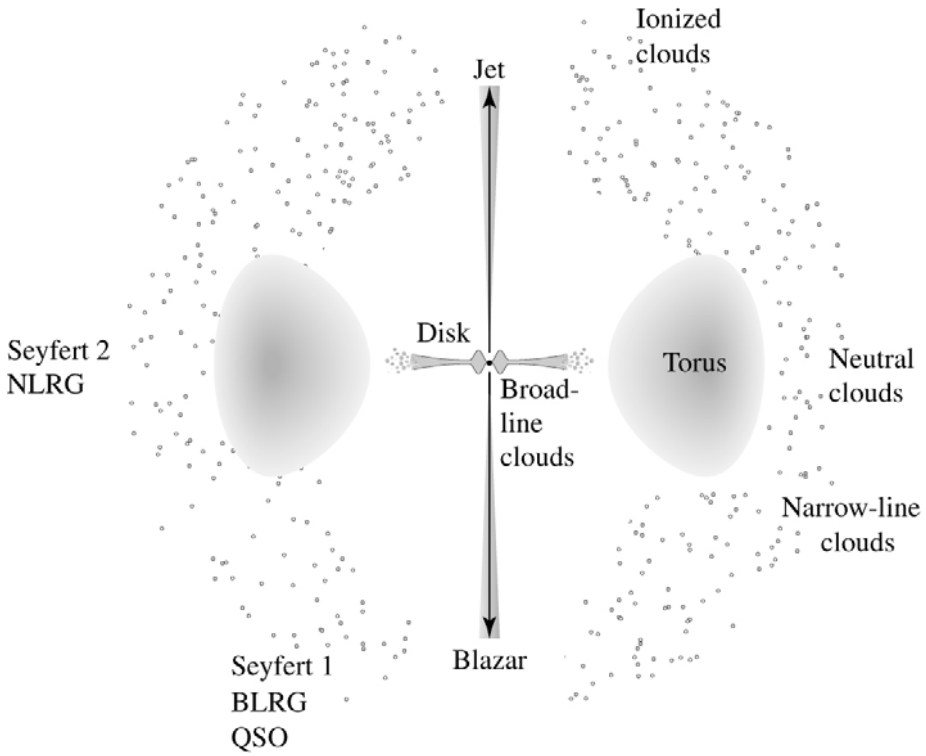

Figure 3.1: A sketch of the cross section of an active galactic nucleus. The relative observation positions for various types of AGN are shown along with the different components making up AGN. Image courtesy of Carroll and Ostlie (2007).

and Matthews, 1963). Hubble's Law indicates that this object should have a distance of roughly 5×10^9 ly, and a luminosity of 1.5×10^{12} $L_\odot = 5.6 \times 10^{38}$ W.

Quasars have been subsequently linked to active galactic nuclei (AGN), which eject huge amounts of gas in two jets that extend in opposite directions away from their home galaxy. AGN are created when a large amount of gas forms an accretion disk around a supermassive black hole. Accretion disk particles eventually form two jets, directed perpendicular to the accretion disk, which are ejected through interactions with the central supermassive black hole. More specifically, these particles are thought to be accelerated along the magnetic field lines created in the interaction between the accretion disk and the rotating black hole, which, in the near vicinity of the black hole, are directed towards and away from its south and north magnetic poles, respectively (Carroll and Ostlie, 2007). Because the electrons and positrons in these energetic jets are accelerated to speeds near c, this mechanism is capable of generating very bright synchrotron radiation. Thus, quasars with large accretion disks fueling these jets would be extremely luminous. Nearby AGN, however, usually contain a relatively small accretion disk with low luminosity jets. This is likely due to the depletion of accretion disk fuel for AGN over the history of the universe. We observe many different types of AGN, depending on their orientation relative to us (see Figure 3.1).

Quasars are thought to be the precursors of blazars and Seyfert 1 galaxies; AGN whose jets

are directed almost exactly in our direction. In the early universe, galaxies would have contained an abundance of fuel, which has since been diminished through processes in stars and AGN. With large amounts of fuel, AGN would have been extremely bright. As it turns out, these objects were so bright that we can see them at distance scales as large as the observable universe. The finite speed of light, therefore, implies that we can use quasars to gain understanding of the evolutionary history of the universe from a time when the first structures were being formed.

This model for quasars is widely accepted because it explains all of the observed phenomena. Black holes – even supermassive black holes – take up a very small area in space. The spacetime geometry outside a spherically symmetric mass is given by the Schwarzschild geometry,

$$ds^2 = -\left(1 - \frac{2GM}{c^2 r}\right)(cdt)^2 + \left(1 - \frac{2GM}{c^2 r}\right)^{-1} dr^2 + r^2\left(d\theta^2 + \sin^2\theta d\phi^2\right). \tag{3.1}$$

From this geometry, the radius of the event horizon of a Schwarzschild black hole, inside which light can only move radially inward, is

$$R_S = \frac{2GM}{c^2}. \tag{3.2}$$

For even the most massive black holes this radius is nowhere near the maximum radii we calculate from quasar light curves. Furthermore, according to AGN theory these objects should be so bright that even the large distances we infer from their redshifts are not unreasonable. Finally, the large distances to quasars gives the resolution to why quasars should be located mainly near galaxies. Even though quasars are very bright, we still would not see as many of them as we do if not for a process known as *gravitational lensing*. If a massive object, such as a galaxy or a cluster of galaxies, is situated between us and a more distant, luminous object, the light from the more distant object will be bent around the massive object by the curvature of space. This process actually helps to brighten the quasar as we see it and, in fact, can sometimes produce multiple images of the same quasar around the massive object. If quasars were not very far from us, they would not be able to be gravitationally lensed by intermediate galaxies. Thus, observations of gravitational lensing have served two purposes: they support the distances we infer through Hubble's Law and they provide a reason for the observed preference of quasars to be near galaxies and galaxy clusters.

3.2 Calculating Cosmological Distances

The first element needed in the analysis of any astronomical data is the *luminosity distance*; a distance measure which has the advantage of being directly inferred from the measured flux of an object. From the Robertson-Walker metric we can calculate the circumference of a circle of radius r at time t as

$$\int_0^{2\pi} d\phi\sqrt{g_{\phi\phi}} = 2\pi a(t) r \tag{3.3}$$

and the area of a sphere with radius r as

$$\int_0^\pi d\vartheta \int_0^{2\pi} d\phi \sqrt{g_{\vartheta\vartheta} g_{\phi\phi}} = \int_0^\pi d\vartheta \int_0^{2\pi} d\phi a^2(t) r^2 \sin(\vartheta) = 4\pi a^2(t) r^2. \tag{3.4}$$

We denote the distance

$$d_A = a_0 r \tag{3.5}$$

as the current *angular diameter distance*. However, for curved spacetimes this distance is not the actual physical distance. We calculate the *physical distance* from our location at $r = 0$ to an object a radial distance r from us as

$$d = \int_0^r dr \sqrt{g_{rr}} = a(t) \int_0^r d\chi = \begin{cases} a(t) \ln(r + \sqrt{1 + r^2}) & k = -1 \\ a(t) r & k = 0 \\ a(t) \arcsin(r) & k = 1 \end{cases}. \tag{3.6}$$

The angular length coordinate r can thus be calculated as a function of the radial length coordinate χ:

$$r = \frac{1}{\sqrt{k}} \sin\left(\sqrt{k}\chi\right) = \begin{cases} \sinh(\chi) & k = -1 \\ \chi & k = 0 \\ \sin(\chi) & k = 1 \end{cases}. \tag{3.7}$$

However, a more useful distance in cosmology because it can be measured through observations of objects of known luminosities is the luminosity distance

$$d_L \equiv \sqrt{\frac{L}{4\pi f}}. \tag{3.8}$$

The photons we receive from an object today are distributed over an area $4\pi a_0^2 r^2$. Their energy will have decreased by a factor $(1 + z)^{-1}$ and they will be thinned out in the longitudinal direction by a factor $(1 + z)^{-1}$. The flux we receive from an object with luminosity L should then be given by

$$f = \frac{L}{4\pi a_0^2 r^2 (1 + z)^2}. \tag{3.9}$$

The luminosity distance is then

$$d_L = (1 + z) d_A = (1 + z) \frac{a_0}{\sqrt{k}} \sin\left(\sqrt{k}\chi\right) = (1 + z) \frac{a_0}{\sqrt{k}} \sin\left(\sqrt{k} \frac{d}{a_0}\right). \tag{3.10}$$

Now let us suppose we observe a quasar at comoving coordinates $\{r, \vartheta, \phi\}$. From the Robertson-Walker metric we obtain

$$\dot{\chi}(t) \equiv \frac{\dot{r}(t)}{\sqrt{1 - kr^2}} = -\frac{1}{a(t)} \tag{3.11}$$

for the radial length coordinate. Thus, we obtain the present physical distance to the quasar's position when the light was emitted

$$\begin{aligned} d &= a_0 \chi = a_0 \int_0^\chi d\chi = a_0 \int_{t_0}^{t_e} dt \dot{\chi}(t) = a_0 \int_{t_e}^{t_0} \frac{dt}{a(t)} = a_0 \int_{a_e}^{a_0} \frac{da}{a\dot{a}} \\ &= -\int_{a_0/a_e}^1 \frac{a}{\dot{a}} d\left(\frac{a_0}{a}\right) = a_0 \int_1^{1+z} \frac{du}{u\dot{a}}. \end{aligned} \tag{3.12}$$

We can now use (2.42) to find d in terms of the redshift

$$d(z) = \frac{1}{H_0}\int_1^{1+z} \frac{du}{\sqrt{\Omega_R u^4 + \Omega_M u^3 + (1-\Omega_M-\Omega_R-\Omega_\Lambda)u^2 + \Omega_\Lambda}}. \tag{3.13}$$

This formula can be simplified by recognizing that the current radiation density, $\Omega_R \ll \Omega_M \lesssim \Omega_\Lambda$, is negligible compared to the matter and vacuum densities. Thus, we obtain the current cosmological physical distance

$$d(z) = \frac{1}{H_0}\int_1^{1+z} \frac{du}{\sqrt{\Omega_M u^3 + (1-\Omega_M-\Omega_\Lambda)u^2 + \Omega_\Lambda}} \tag{3.14}$$

and the luminosity distance

$$\begin{aligned} d_L(z) &= (1+z)\frac{a_0}{\sqrt{k}}\sin\left(\sqrt{k}\frac{d}{a_0}\right) \\ &= \frac{1+z}{H_0\sqrt{\Omega_M+\Omega_\Lambda-1}}\sin\left(\int_1^{1+z} du \frac{\sqrt{\Omega_M+\Omega_\Lambda-1}}{\sqrt{\Omega_M u^3 + (1-\Omega_M-\Omega_\Lambda)u^2+\Omega_\Lambda}}\right), \end{aligned} \tag{3.15}$$

where in the second line (2.43) has been used to eliminate the factor of $a_0/\sqrt{k}$.

This analysis has been done in units where $c = 1$. Inserting c in its proper place, we find

$$d_L(z) = \frac{c(1+z)}{H_0\sqrt{\Omega_M+\Omega_\Lambda-1}}\sin\left(\int_1^{1+z} du \frac{\sqrt{\Omega_M+\Omega_\Lambda-1}}{\sqrt{\Omega_M u^3 + (1-\Omega_M-\Omega_\Lambda)u^2+\Omega_\Lambda}}\right), \tag{3.16}$$

from which we make use of $\lim_{x\to 0}\sin\alpha x/x = \alpha$ and $\sin(ix) = i\sinh(x)$ to explicitly write the cases $\Omega_M + \Omega_\Lambda = 1$ and $\Omega_M + \Omega_\Lambda < 1$.

3.3 Apparent Magnitudes from Quasar Observations: the K-correction

The term apparent magnitude was introduced in §3.1 as a unit of brightness. In this section I will provide a brief description of the magnitude scale en route to the final element needed for a useful interpretation of high redshift data; the K-correction.

In the second century B.C., Hipparchus invented the magnitude scale to describe the apparent brightness of stars in the sky. The brightest stars were given a magnitude value of $m = 1$, while the dimmest stars were given a magnitude of $m = 6$. The modern definition of the magnitude scale is that a difference of 5 magnitudes corresponds to a difference in brightness of 100 (Carroll and Ostlie, 2007). The standard reference point for the magnitude scale is the magnitude of Vega measured over all wavelengths (its *bolometric magnitude*), which is set to $m_{bol} = 0$. With this definition, we find that two stars with magnitudes m_1 and m_2 will have a flux ratio of

$$\frac{f_2}{f_1} = 100^{(m_1-m_2)/5}. \tag{3.17}$$

This definition helps when comparing magnitudes of objects as seen from earth; however, it does not help us describe the geometry of the universe because insertion of (3.8) into (3.17) for two

objects leaves too many unknowns. To aid us in a description of our universe we need a way of comparing the apparent magnitude of an object to its intrinsic brightness. This is accomplished with the definition of *absolute magnitude*, M; the apparent magnitude of an object if it were located at a distance of 10 parsecs (pc). Using this definition, we combine (3.8) and (3.17) to obtain the relationship between luminosity distance, apparent magnitude, and absolute magnitude:

$$m - M = 5 \log_{10} \left(\frac{d_L}{d_0} \right), \tag{3.18}$$

where $d_0 \equiv 10$ pc. The left hand side of (3.18) is normally called the object's *distance modulus* and (3.18) is known as the distance modulus equation.

Now we have a very nice equation relating apparent and absolute magnitudes of an object to its luminosity distance; and thus, due to (3.15), to the FRW parameters. Therefore, (3.18) implies that if we are able to measure the apparent bolometric magnitudes of a set of *standard candles* (objects with known absolute bolometric magnitudes) we should be able to determine values for the cosmological parameters.

Unfortunately we still live in a world where most astronomical observations have to be made with ground based telescopes. Because of Earth's atmosphere, astronomers prefer to make their observations with optical filters (see Figure 3.2). The primary reason for this is that filters can be

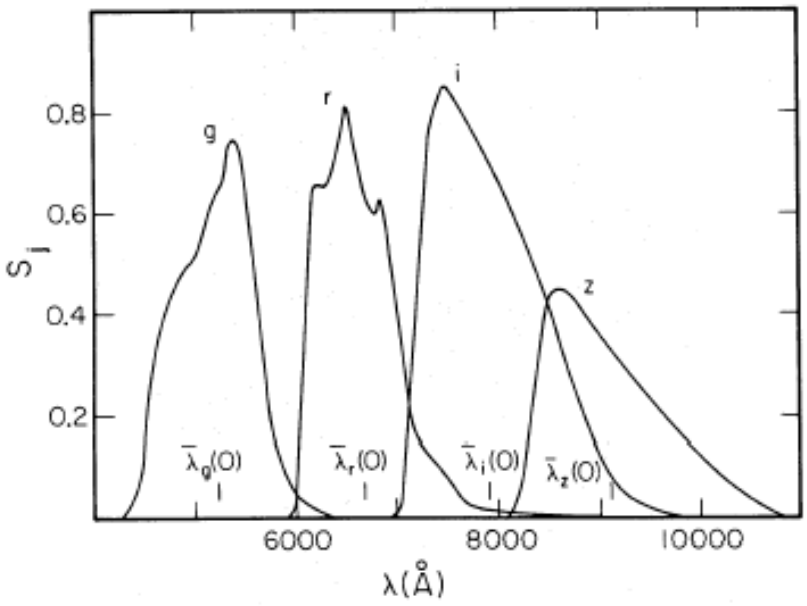

Figure 3.2: Transmission function $S_j(\lambda)$ for the bandpasses of the *griz* system taken from Schneider *et al.* (1983). The SDSS uses a similar system whose *griz* transmission functions are slightly different due to their different instrumentation. As well, they have added a u filter to their observations which has a peak transmission wavelength of 3541 Å (Schneider *et al.*, 2002). For reasons stated in §4.1, we will be primarily interested in i band measurements in the analysis of the SDSS DR3 data, thus future discussion will focus only on the i band.

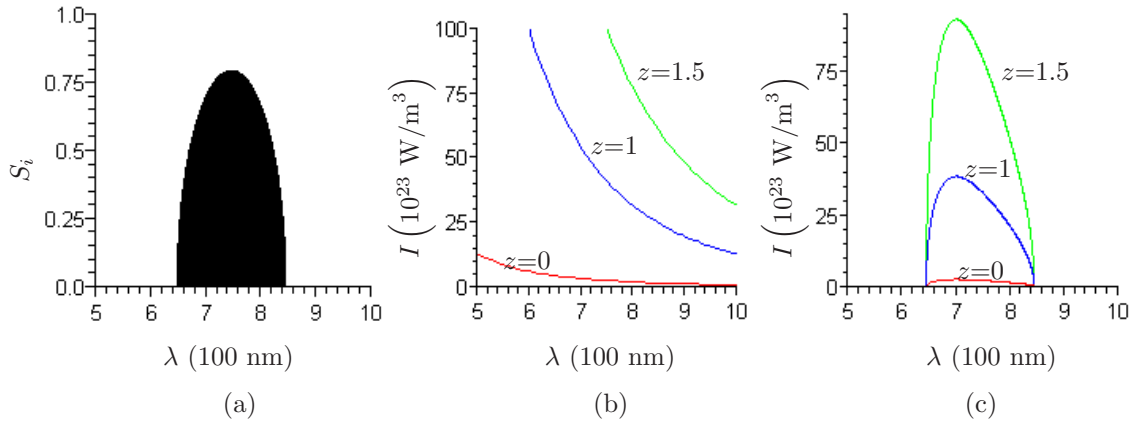

Figure 3.3: (a) An idealized i band transmission function defined by the half-ellipse $S_i(\lambda) = 0.8\sqrt{1 - \frac{(\lambda - 746\ \mathrm{nm})^2}{(100\ \mathrm{nm})^2}}$. (b) Planck's radiation law, $I(\lambda, 10^6\ \mathrm{K}) = \frac{2hc^2}{\lambda^5} \frac{1}{e^{hc/(\lambda k_B 10^6\ \mathrm{K})} - 1}$ in the region of the i band for redshifts $z = 0, 1$, and 1.5. (c) The product $S_i(\lambda) \cdot I(\lambda, 10^6\ \mathrm{K})$ whose integration leads to the determination of the apparent magnitude.

used to avoid detection of strong atmospheric spectral lines. However, a problem arises when we make observations of high redshift objects with filters; the data which are being observed have been redshifted *into* the wavelength band of the filter (see Figure 3.3). Thus, highly redshifted quasars will appear much brighter in a given wavelength band because they emit most of their light as γ- and X-rays and most ground based astronomy is accomplished through observations of visual and infrared light. This problem is the source of the previously mentioned K-correction.

Following the notation of Schneider *et al.* (1983), the transmission function for each filter j as a function of frequency ν is defined to be $S_j(\nu)$. If we define $N_{\nu(1+z)}$ to be the number of photons emitted from our source at a redshifted frequency $\nu(1+z)$, then the number of incident photons with frequency ν per unit time and area is given by

$$n_\nu = \frac{N_{\nu(1+z)}(1+z)^2}{4\pi d_L^2}, \tag{3.19}$$

from which the apparent magnitude is defined to be

$$m_j = C_j - 2.5 \log_{10} \left(\int_0^\infty d\nu \frac{N_{\nu(1+z)}(1+z)^2 S_j(\nu)}{4\pi d_L^2} \right), \tag{3.20}$$

where C_j is a constant to be "found from photometric standards" (Schneider *et al.*, 1983). Inserting the definition of absolute magnitude into (3.20), we obtain

$$M_j = C_j - 2.5 \log_{10} \left(\int_0^\infty d\nu \frac{N_\nu S_j(\nu)}{4\pi d_0^2} \right). \tag{3.21}$$

Finally, the K-corrected distance modulus equation for redshifted objects is given by the subtraction of (3.21) from (3.20):

$$m_j - M_j = 5 \log_{10} \left(\frac{d_L}{d_0} \right) + 2.5 \log_{10} \left(\frac{1}{(1+z)^2} \frac{\int_0^\infty d\nu N_\nu S_j(\nu)}{\int_0^\infty d\nu N_{\nu(1+z)} S_j(\nu)} \right)$$

$$= 5\log_{10}\left(\frac{d_L}{d_0}\right) + 2.5\log_{10}\left(\frac{1}{1+z}\frac{\int_0^\infty d\nu(f_\nu/\nu)S_j(\nu)}{\int_0^\infty d\nu(f_{\nu(1+z)}/\nu)S_j(\nu)}\right). \tag{3.22}$$

For quasars, this equation can be simplified by noting that for certain redshift ranges their spectra can be well approximated by a power law:

$$f_\nu \propto \nu^\alpha \tag{3.23}$$

(Vanden Berk *et al.*, 2001). Substituting this expression into (3.22) yields

$$m_j - M_j = 5\log_{10}\left(\frac{d_L}{d_0}\right) - 2.5(1+\alpha)\log_{10}(1+z) \tag{3.24}$$

for each filter j. Tests using SDSS quasars indicate that at emission wavelengths below 5000 Å (our eventual region of interest) this power law frequency continuum index has a value of $\alpha \approx -0.5$ (Vanden Berk *et al.*, 2001).

Chapter 4

Analytical Framework for Tests Involving Large Catalogues of Quasars

The most reliable tests that have directly measured both Ω_M and Ω_Λ have used observations of SNe Ia as standard candles. A SN Ia is the dramatic explosion of a white dwarf star as it accretes enough mass from a binary companion to exceed the 1.4 $M_\odot$ Chandrasekhar limit and explosively ignite carbon fusion. Because of the exact nature of these explosions they have very distinct light curves and are thus very accurate standard candles. Indeed, recent observations designed to test contaminants to SNe Ia data such as luminosity evolution, gray intergalactic dust, gravitational lensing, and selection bias indicate that SNe Ia act as very reliable standard candles (Tonry *et al.*, 2003; Foley *et al.*, 2007).

Because SNe Ia light curves are in fact presumed to be universal, observations of these objects have provided the only reliable, independent means of measuring Ω_Λ. Indeed, as Tonry *et al.* (2003) note, CMB observations imply a total energy density, $\Omega_0 = 1.00 \pm 0.02$ and galaxy cluster measurements imply $\Omega_M \approx 0.3$ (see Spergel *et al.*, 2003; Colless *et al.*, 2001); thus, according to the Λ CDM big bang model, any reliable observation which directly measures Ω_Λ should result in a value of ~ 0.7.

Recent measurements of the CMB anisotropy signature by WMAP have strengthened the estimates provided by SNe Ia and other sources. However, the WMAP results are not independent, due to the use of Bayesian statistical analysis, and are thus subject to the limitations of hypotheses which are based on prior measurements. A detailed description of the original parameter estimation methodology used by the WMAP team may be found in Verde *et al.* (2003). Only minor changes to these methodologies have been implemented during the analysis of the three-year results (Spergel *et al.*, 2007).

One issue that is encountered with observations of SNe Ia is that their peak brightness is dimmer than $M_{bol} = -20$, so they have only been detected in great numbers out to redshifts slightly greater than $z \approx 1$, corresponding to a lookback time of 7.6 Gyr (Astier *et al.*, 2006; Riess *et al.*, 2007). Conversely, the brightest quasars have absolute bolometric magnitudes of roughly $M_{bol} = -30$ (10^4 times brighter than a SN Ia – allowing for quasar observations out to $z > 6$) less than 1Gyr after

the big bang. We have seen previously that for an $\Omega_M = 0.24$, $\Omega_\Lambda = 0.76$ geometry, the universe began to accelerate at $z_{accel} = 0.85$ (see (2.46)), which corresponds to a lookback time of ~ 7 Gyr. Therefore, the majority of observed SNe Ia occurred during the acceleration era and so, provide little direct evidence for the rate of expansion of the universe during the matter dominated era.

In the present analysis, quasars will be used to perform an independent test to determine Ω_M and Ω_Λ. Quasars are bright enough that they have been observed in appreciable numbers out to $z \approx 5$, so they may be used to directly analyze the state of the universe at times well within the matter dominated era. The final data set used in this analysis will contain quasars with redshifts in the range $3 \leq z \leq 5$; thus we will be analyzing data only from the alleged decelerating, matter dominated era.

Unfortunately, this analysis is also not free of assumptions. Thus far, we have employed three assumptions in the design of our physical model: (i) we have assumed a dark energy equation of state, $p_\Lambda = w\rho_\Lambda$, with $w = -1$, which is consistent with a time-independent Λ and the recent WMAP and SNe Ia results (Astier *et al.*, 2006; Riess *et al.*, 2007; Spergel *et al.*, 2003; Spergel *et al.*, 2007), (ii) we have opted to neglect Ω_R, based on arguments involving the COBE results (Mather *et al.*, 1999), and (iii) we have assumed that quasar spectra obey a power law frequency distribution given by (3.23), which is standard in quasar analyses (Vanden Berk *et al.*, 2001; Schneider *et al.*, 2007). The first two assumptions are the basic components of the Λ CDM model, which has become the standard model in cosmology over the past decade. This model is known as the Λ CDM model because it incorporates the cosmological constant and cold dark matter (CDM) as the primary energy density components in the universe. In §§4.2 and 4.3, two final assumptions, specific to the analysis of quasars in this project, will be described.

4.1 The SDSS Quasar Catalogue

The data used in this thesis will be the quasars from the SDSS DR5 value added catalogue (hereafter, the Catalogue) (Schneider *et al.*, 2007). The SDSS quasars have all been discovered using a dedicated 2.5 m f/5 modified Ritchey-Chretien altitude-azimuth telescope located at Apache Point Observatory, in south east New Mexico. This telescope has a 1.08 m secondary mirror and two corrector lenses, which result in a 3° distortion-free field of view (York *et al.*, 2000). After making numerous algorithmic cuts to the DR5 data to remove possible stars, galaxies, etc., the spectra of the objects in the Catalogue were examined individually so that out of the $\approx 10^6$ objects in DR5, the Catalogue boasts 77 429 objects identified as quasars to a high degree of confidence (see Figure 4.1).

For the remainder of this analysis, we will be using i band apparent magnitudes. Normally, absolute magnitudes are calculated using B filter measurements. The SDSS quasar point-spread

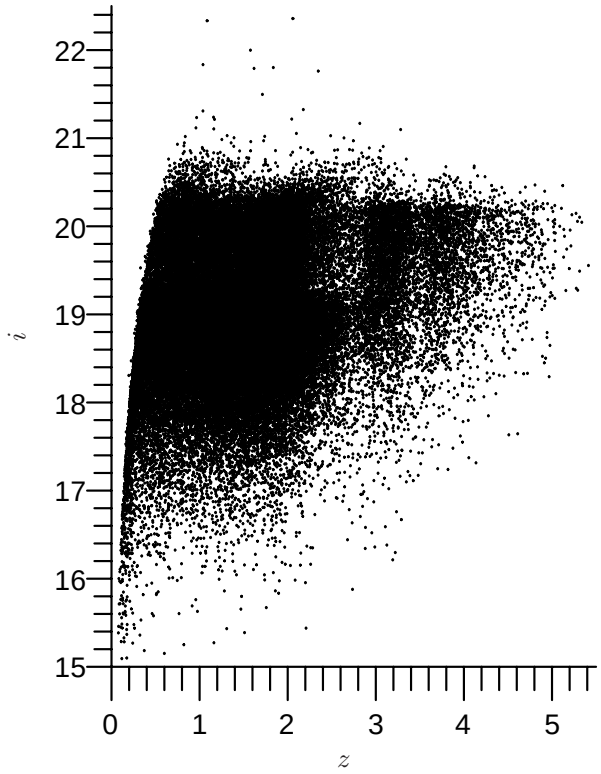

Figure 4.1: All quasars in the Catalogue plotted in the $i - z$ plane. Noticeable features of this plot, such as the sharp cutoff in quasars at low redshifts, the less dramatic cutoffs in number density at $i \approx 19.1$ when $z \lesssim 3$ and $i \approx 20.2$ when $z \gtrsim 3$, as well as at $z \approx 2.7$ and $z \approx 3.5$ will be discussed in § 4.3. The minimum apparent magnitude allowed in the selection algorithms used by Schneider *et al.* (2007) was 15.

function (PSF) magnitudes are derived from observations using u, g, r, i, and z filters, which have effective bandpass wavelengths of 3541, 4653, 6147, 7461, and 8904 Å, respectively (Schneider *et al.*, 2007). For the compilation of the SDSS quasar catalogues, the i band was selected to be the luminosity indicator. This is because in highly redshifted spectra, the Lyα emission line may be redshifted past many filters, resulting in unreliable measurements due to the absorption produced by the Lyα forest and Lyman limit systems. Thus, the i filter is appropriate to use in quasar analysis because the Lyα line only reaches its centre at $z \approx 5$ (Schneider *et al.*, 2002).

The Catalogue also contains galactic extinction values for each object. Because the quasars we are using in this analysis were observed in different areas of the sky, the amount of light scattered due to intermediate dust particles will be different for each quasar. The u band galactic extinction coefficients A_u were determined by the SDSS from the maps of Schlegel *et al.* (1998). The i band extinction coefficients are simply calculated using $A_i = 0.405 A_u$ (Schneider *et al.*, 2007). The galactic extinction corrected i band apparent magnitude (hereafter, the "apparent magnitude") is

defined here as

$$m_i \equiv i - A_i, \tag{4.1}$$

where i is the measured apparent magnitude in the i band.

Figure 4.1 contains all the quasars in the Catalogue plotted in the $i - z$ plane. By visual inspection, we see that quasars cannot be used as standard candles in the same way as SNe Ia because at every redshift there is a continuum of magnitudes that is apparently only cut off on the high end by the magnitude limits of the study. Furthermore, luminosity evolution of the various subspecies of quasars must also be considered. For these reasons, we will use only the brightest quasars within small redshift bins and incorporate a parameter for luminosity evolution into our model.[1]

To this end, we determine the optimal size to use for the redshift bin width by minimizing the function

$$\Sigma(\Delta z) \equiv \frac{1}{N(\Delta z) - 1} \sum_{j=2..N(\Delta z)}^{N(\Delta z)} \left| m_{i,\min}(Z_j) - m_{i,\min}(Z_{j-1}) \right|, \tag{4.2}$$

where N is the total number of redshift bins with width Δz, Z_j is the jth redshift bin, and $m_{i,\min}$ is its minimum apparent magnitude. The width Δz_{opt} which minimizes this summation will provide us with the optimum statistical distribution of quasars within each bin by ensuring two things:

i. The bins must be wide enough that the apparent magnitude minima are not too scattered due to small sample sizes, and

ii. The bins must be narrow enough that the effects of luminosity evolution and observational bias (apparent magnitudes of closer quasars will be brighter due to the inverse square law for light) are negligible at the scale of the bin width.

Evaluations of $\Sigma(\Delta z)$ for discrete bin widths have been plotted in Figure 4.2. This calculation implies the optimal bin width is $\Delta z_{\text{opt}} = 0.09$ when using quasars with $z \geq 2$.

Choosing the optimal bin width in this manner provides our data set with two important properties which will be utilized in the upcoming analysis:

i. The redshifts of the minimum apparent magnitudes will be uniformly distributed about the midpoints z_j of their respective bins Z_j, allowing us to use the midpoints of each bin as z values in a curve fitting analysis, and

ii. The redshifts of all the quasars in any bin will be approximately uniformly distributed; thus, the apparent magnitude values in each bin should all be drawn from the same distribution.

[1] Note that at redshifts below $z \approx 2$, the brightest quasars in the population may have been cut off by the $m_i \geq 15$ minimum magnitude limit of the study, which has been imposed to avoid confusion with stars. For this reason, we will begin this analysis using only quasars with $z \geq 2$.

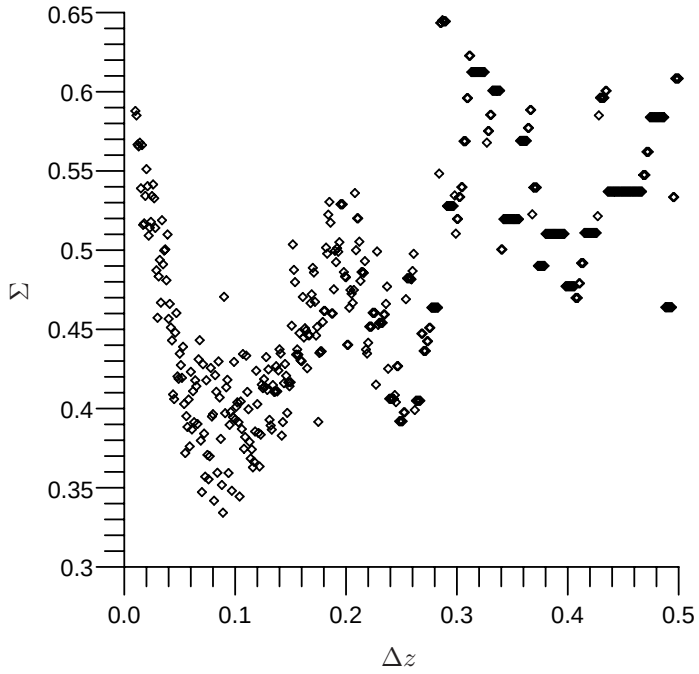

Figure 4.2: $\Sigma(\Delta z)$ from all quasars in the Catalogue with $z \geq 2$ calculated for redshift widths in the range $0.01 \leq \Delta z \leq 0.5$ with a resolution of 10^{-3}. The optimal bin width $\Delta z_{\rm opt} = 0.09$ determined by this calculation was used in a qualitative analysis of the luminosities of the apparent magnitude minima in order to determine a more appropriate redshift minimum for this analysis.

4.2 Quasar Luminosity Evolution

In this section, we will modify the distance modulus equation by adding a luminosity evolution term so that we may eventually determine values for the cosmological parameters by fitting to the brightest quasars in the Catalogue.

According to galaxy evolution theories, quasars would have begun to form at roughly the same time as galaxies. The luminosity of the brightest quasars would have increased statistically as the total number of quasars increased, as well as systematically as the sizes of their supermassive black hole engines began to increase following their first formation. To further complicate issues, the mixing of gas during galaxy mergers is also thought to be linked to quasar formation. However, as galaxies have moved further apart and quasars have used up significant amounts of their fuel, the numbers and average luminosities of quasars have decreased.

This paints a very complex picture for luminosity evolution, which we will attempt to simplify with the choice of an appropriate redshift range. In particular, we will try to capture the rise of the quasar luminosity shortly following first formation.

To begin with, we use a qualitative assessment to determine a more precise lower limit to the redshift range, based on whether or not the quasar luminosities may be modeled with a simple

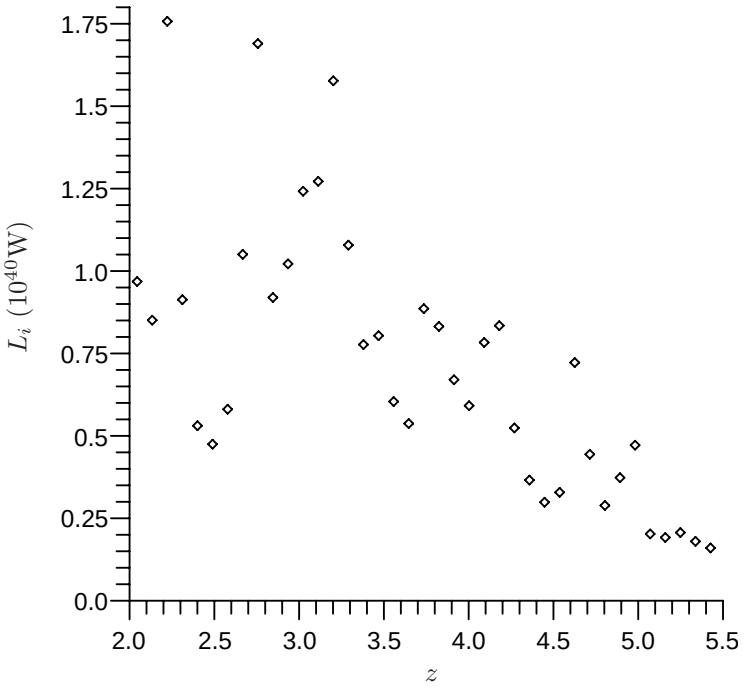

Figure 4.3: Luminosities of brightest quasars with $z \geq 2$ in bins of width $\Delta z = 0.09$. Data in the range $2 \leq z \leq 2.6$ appear much too scattered and have been removed from further analysis.

function. Figure 4.3 is a plot of the luminosities[2] of all the brightest quasars with $z \geq 2$ from redshift bins of width $\Delta z = 0.09$. From this plot, it appears that in the range $2.0 \leq z \leq 2.6$ the luminosities of the brightest quasars did not follow the same trend, as values began to fall off the strictly increasing path. Quasars in this range would not be useful in our analysis because these magnitude values are likely the result of an overall drop in the availability of fuel to quasars, with an occasional bright value due to mixing from processes such as galactic mergers. The overall effect is that the apparent magnitude minima in this redshift range are too scattered and their influence should thus be removed from the determination of Δz_{opt}. Therefore, the values of $\Sigma(\Delta z)$ have been recalculated using only quasars with $z \geq 2.6$ (see Figure 4.4). The result is that the optimal bin width to use in our analysis is $\Delta z_{\text{opt}} = 0.096$.

At this point we have minimum apparent magnitude and redshift values for redshift bins of an appropriate width and we may now use these data to aid in determining an appropriate luminosity evolution equation. The most computationally simplistic luminosity evolution we can use is

$$L(z) = L_0(1+z)^{\beta}, \tag{4.3}$$

where $L_0 \equiv L(z=0)$, because the constant parameter β is completely degenerate with α in the

[2]The luminosity values plotted in this image have been calculated using the current literature parameter values $H_0 = 73$ (km/s)/Mpc, $\Omega_M = 0.24$, $\Omega_\Lambda = 0.76$, and $\alpha = -0.5$ (Spergel *et al.*, 2007; Vanden Berk *et al.*, 2001). These values will be used in the remainder of the luminosity calculations in this section.

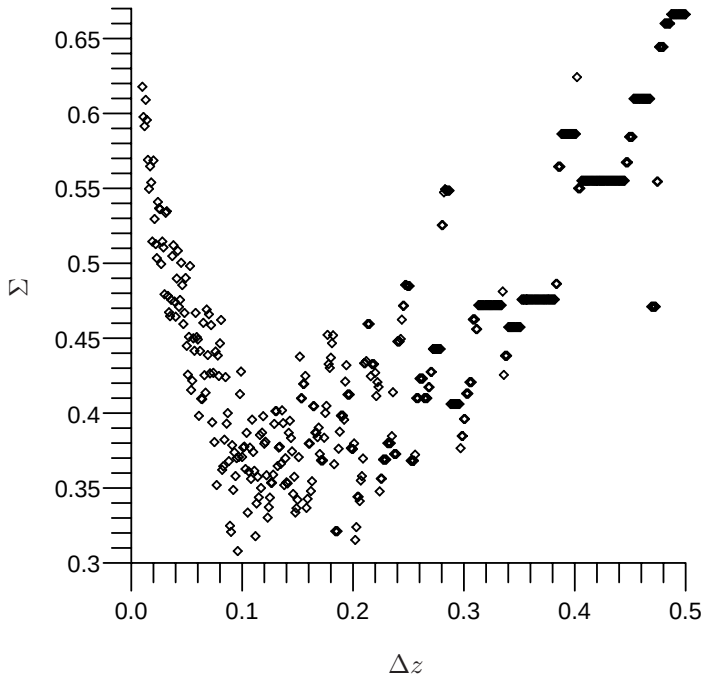

Figure 4.4: $\Sigma(\Delta z)$ from all quasars in the Catalogue with $z \geq 2.6$ calculated for redshift widths in the range $0.01 \leq \Delta z \leq 0.5$ with a resolution of 10^{-3}. The optimal bin width which will be used in the remainder of the analysis is $\Delta z_{\rm opt} = 0.096$.

K-correction described in § 3.3. To see this degeneracy, we note that (3.17) can be expressed as

$$M_2 = M_1 - 2.5 \log_{10} \left(\frac{L_2}{L_1} \right) \tag{4.4}$$

for two arbitrary luminous objects. Therefore, if we substitute (4.3) into (4.4) we find that the absolute magnitude of an object with continuous luminosity evolution described by (4.3) should evolve according to

$$M(z) = M_0 - 2.5\beta \log_{10}(1+z), \tag{4.5}$$

where $M_0 \equiv M(z=0)$. Thus, once we have found an appropriate redshift range for which we can model the luminosity evolution of quasars using (4.3), we may modify the distance modulus equation (3.24) for i band magnitudes to

$$m_i - M_{i,0} = 5 \log_{10} \left(\frac{d_L}{d_0} \right) - 2.5(1+\alpha+\beta) \log_{10}(1+z). \tag{4.6}$$

Unfortunately, establishing a degeneracy between the k-correction and a possible form of luminosity evolution is not justification enough for using such an equation. However, we do not want to include too many parameters in our curve fit which may be strongly covariant. Therefore, for this project we will content ourselves with showing that (4.3) should be general enough to model the apparent magnitude minima in some redshift range. Figure 4.5 is a plot of the luminosities of the brightest quasars with $z \geq 2.6$ from redshift bins of width $\Delta z = 0.096$, together with (4.3)

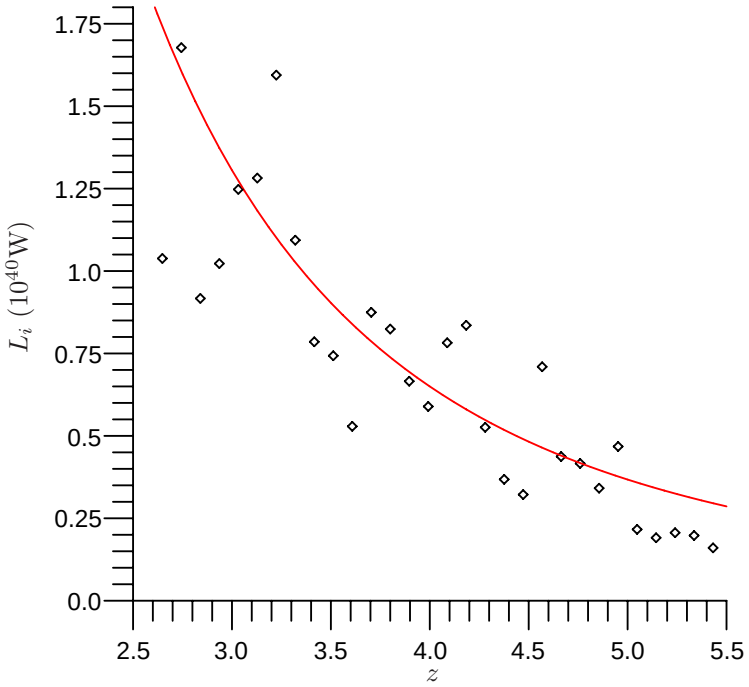

Figure 4.5: Luminosities of brightest quasars with $z \geq 2.6$ in bins of width $\Delta z = 0.096$. The best fit luminosity evolution curve, with $\beta = -3.13$, shown in red was calculated using only the data in the range $3 \leq z \leq 5$.

evaluated for the parameter values which best fit the luminosities in the range $3 \leq z \leq 5$.[3] This plot shows that (4.3) fits these data fairly well. Therefore, we may conclude that not only should this function be appropriate to use – at least as a preliminary guess – in this analysis, but if we wish to keep the power law frequency continuum index, α, as a free parameter in our model we should not use any other luminosity evolution parameter because it would inevitably be highly covariant with α, introducing a large degree of uncertainty in the final fitted parameters.

Therefore, the assumption that the luminosity of early quasars evolved according to (4.3) appears to lead to the simplest model we can use in our analysis while keeping all the Λ CDM parameters free, which should lead to the best results providing β is not strongly covariant with the density parameters we are hoping to determine.

Another argument in favour of using (4.3) is that it has been argued in the literature that the luminosity evolution of any particular species of galaxies in which only internal processes (i.e. stellar evolution, with no significant merging) are responsible for increases in luminosity with increasing redshift may be modeled this way (Jackson and Dodgson, 2002). Although in this analysis, we are looking at high redshift quasars with luminosities that decrease with increasing redshift, we may still assume that during the early stages of galaxy formation the luminosity of the brightest quasars

[3]This range was used in determining the parameter values used when plotting (4.3) because in the final analysis a χ^2 minimization of (4.6) to the data in $3 \leq z \leq 5$ has the lowest reduced χ^2 value of any redshift range within $2.6 \leq z \leq 5.5$.

grew at a fairly smooth rate, according to increasing supermassive black hole mass. We have already argued in this section that at redshifts below $z \approx 2.6$ the fuel for quasars must have begun to deplete because the luminosities of the brightest quasars at these redshifts become more scattered, likely only reaching their maximum potential during mergers when large amounts of gas and dust would enter the vicinities of the largest supermassive black holes. Therefore, the luminosity evolution of these brightest quasars may be similar in effect to that of low redshift galaxies, which have dimmed at a fairly uniform rate due to stellar evolution.

4.3 Error Bars for the Most Luminous Quasars

Eventually, we would like to fit (4.6) to the most luminous quasars in the Catalogue by performing a χ^2 minimization. That is, we would like to determine the parameters $\mathbf{A}$ which minimize the quantity

$$\chi^2(\mathbf{A}) = \sum_{j=1}^{N} \left[\frac{m_{i,\min,j} - m_i(z_j; \mathbf{A})}{\sigma_j} \right]^2 , \tag{4.7}$$

where σ_j is the error associated with the data point $m_{i,\min,j}$ with redshift z_j. In the previous section, we determined a statistical sample of the brightest SDSS DR5 quasars; however, we still have a few tasks to perform before we may find the parameter values which minimize (4.7). Specifically, we must determine the errors associated with the use of the minimal apparent magnitudes from each redshift bin in this analysis, then we will formulate the luminosity distance (3.15) in terms of normal elliptic integrals so that values of (4.7) and its derivative with respect to $\mathbf{A}$ may be evaluated efficiently for varying parameter values, and finally, we will determine degeneracies between some of the constant parameters in our luminosity evolving distance modulus equation (4.6), which will leave four independent parameters for χ^2 minimization.

In this section, we will determine errors associated with the assumption that we actually do have the brightest quasars that could have existed at each redshift. These errors will come from fitting the minimal generalized extreme value distribution (GEVD)

$$F(x; \kappa, \lambda, \delta) = \begin{cases} 1 - \exp\left\{ - \left[1 + \kappa \left(\frac{x-\lambda}{\delta} \right) \right]^{1/\kappa} \right\}, & 1 + \kappa \left(\frac{x-\lambda}{\delta} \right) \geq 0, \text{ if } \kappa \neq 0 \\ 1 - \exp\left[- \exp\left(\frac{x-\lambda}{\delta} \right) \right], & -\infty < x < \infty, \text{ if } \kappa = 0 \end{cases} \tag{4.8}$$

to the apparent magnitudes of all the quasars in each bin separately, and then evaluating the cumulative distribution function (CDF) at the apparent magnitude minimum; thus, determining the probability of the existence of a brighter quasar, as indicated by all quasars in each bin. Therefore, we must ensure that we have a statistical sample – i.e. a representative sample of the $m_i - z$ distribution – of quasars in each bin before we may work out errors.

To this end, let us turn our attention back to Figure 4.1, the plot of all quasars in the Catalogue in the $i - z$ plane. The $m_i - z$ distribution is only slightly altered at the macroscopic level, so

Figure 4.1 will serve our purposes here. In the caption of this image, three non-statistical features of this distribution are mentioned:

i. There is a sharp cutoff curve which is noticeable at $z \lesssim 1$,

ii. There are two drops in number density around $z \approx 2.7$ and $z \approx 3.5$, and

iii. There are also two drops in number density at $m_i \approx 19.1$ for $z \lesssim 3$ and at $m_i \approx 20.2$ for $z \gtrsim 3$.

These features all result from the selection algorithms used by Schneider *et al.* (2007).

The first feature results from the requirement of a maximum absolute magnitude, $M_i = -22$, in the quasar selection algorithms used by Schneider *et al.* (2007), which was calculated using the k-corrected distance modulus equation with $H_0 = 70(\text{km/s})/\text{Mpc},\ \Omega_M = 0.3,\ \Omega_\Lambda = 0.7,$ and $\alpha = -0.5$. This cutoff appears only to affect the distribution of quasars out to $z \lesssim 1$, at which point the flux limit of the SDSS instrumentation becomes the limiting factor.

The decreases in number density at $z \approx 2.7$ and $z \approx 3.5$ are due to the fact that at these redshifts the SDSS colours are similar to those of stars, so many of the possible quasar candidates at these redshifts were taken out of the data set by selection algorithms. At the time of writing, there is no known method for completely removing this feature from the distribution. However, a forthcoming paper detailing the construction of a statistical quasar sample has been promised on the SDSS website (`www.sdss.org`). Therefore, at present we must accept the possibility that error may be incurred in our analysis due to these features. Note, however, that this density gradient is in the z-direction and therefore, because our method of determining an appropriate redshift bin width should have resulted in the most statistically valid apparent magnitude distributions in each bin, this gradient should not have too detrimental an effect on the m_i distributions.

Lastly, the drops in number density at $m_i \approx 19.1$ and $m_i \approx 20.2$ for quasars with $z \lesssim 3$ and $z \gtrsim 3$, respectively, result from the flux limits of the low- and high-z quasar selection algorithms – the two primary algorithms used by Schneider *et al.* (2007) in selecting quasars from the DR5 data. The distribution therefore becomes non-statistical here, and all dimmer quasars must be subtracted from the data set (see Figure 4.6) before the GEVD may be fit to the data, leaving us with only the bright tail of the quasar distribution. This fact turns out to be beneficial because the CDFs of the most common distributions all converge to that of the GEVD in their tails (see Castillo *et al.* (2005), and references therein). Therefore, if we assume that our distribution is close enough to the tail of the actual quasar distribution we may fit the truncated minimal GEVD,

$$F_{X|X\leq x_0}(x;\kappa,\lambda,\delta) = \begin{cases} F_X(x;\kappa,\lambda,\delta)/F_X(x_0;\kappa,\lambda,\delta), & \text{if } x < x_0, \\ 1, & \text{if } x \geq x_0, \end{cases} \tag{4.9}$$

to the apparent magnitudes of all quasars within each bin to determine the errors of our minimal apparent magnitudes *without loss of generality*.

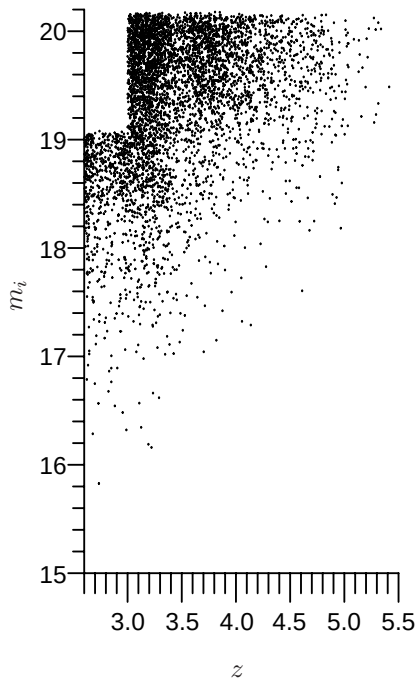

Figure 4.6: $m_i - z$ distribution of quasars with $z \geq 2.6$, which satisfy the minimum flux requirements of the quasar low- and high-z selection algorithms.

This analysis is simplified by individually considering the three distributions which make up the GEVD: the Weibull ($\kappa > 0$), the Reversed Gumbel ($\kappa = 0$), and the Reversed Fréchet ($\kappa < 0$) distributions. Also, by noting that the Reversed Gumbel distribution may be approximated by either the Reversed Fréchet or Weibull distributions by taking $\kappa \to 0$, we find that it is sufficient to fit only these two distributions to the apparent magnitudes. The Weibull distribution is found by substituting $\kappa \to 1/\beta$, $\lambda \to \lambda + \delta$, and $\delta \to \delta/\beta$ for the parameters in (4.8):

$$F_W(x;\beta,\lambda,\delta) = \begin{cases} 0, & \text{if } x < \lambda, \\ 1 - \exp\left[-\left(\frac{x-\lambda}{\delta}\right)^{\beta}\right], & \text{otherwise.} \end{cases} \tag{4.10}$$

Similarly, the substitution of $\kappa \to -1/\beta$, $\lambda \to \lambda - \delta$, and $\delta \to \delta/\beta$ in (4.8) leads us to the common formulation of the Reversed Fréchet distribution:

$$F_F(x;\beta,\delta,\lambda) = \begin{cases} 1 - \exp\left[-\left(\frac{\delta}{\lambda-x}\right)^{\beta}\right], & \text{if } x \leq \lambda, \\ 1, & \text{otherwise} \end{cases} \tag{4.11}$$

(Castillo *et al.*, 2005).

Therefore, both the most likely set of parameters for these distributions, and the distribution from which the apparent magnitudes in each bin were most likely drawn may be determined by maximizing either the likelihood function

$$L(\beta,\delta,\lambda) = \prod_{j=1}^{N} \frac{f(m_{i,j};\beta,\delta,\lambda)}{\delta m_{i,j}}, \tag{4.12}$$

or the log likelihood function

$$\ln(L(\beta,\delta,\lambda)) = \sum_{j=1}^{N} \ln\left(\frac{f(m_{i,j};\beta,\delta,\lambda)}{\delta m_{i,j}}\right), \tag{4.13}$$

where $f \equiv \partial F/\partial x$ has been written for the probability density function (PDF) of either the Weibull or the Fréchet distribution, the weights $1/\delta m_{i,j}$ come from the apparent magnitude measurement errors given in the Catalogue, and N is the number of quasars. Once this has been done, it is a simple matter to evaluate either (4.10) or (4.11) with the best fit parameters to determine statistical errors for the minimal apparent magnitudes.

These values will, however, not entirely account for the errors we require because there is some error associated with the determination of the parameters. A Monte Carlo analysis will be performed to estimate the errors in these parameters. Specifically, we will use the bootstrap method, in which N apparent magnitude values are drawn from the best fit CDF and substituted *with replacement* into the original set of apparent magnitudes. This is done as many times as necessary and subsequent maximum likelihood analyses are used to determine new values for the parameters (Press *et al.*, 1994). The errors in the estimation of the original parameters $(\beta_0, \delta_0, \lambda_0)$ are then estimated from the standard deviations of the bootstrapped parameter values; e.g.

$$\delta\beta = \sqrt{\frac{1}{n_b}\sum_{i=1}^{n_b}(\beta_0 - \beta_i)^2}, \tag{4.14}$$

where n_b is the number of bootstrap iterations, and the error in the CDF evaluation is then calculated from

$$\delta F(m_{i,\min};\beta_0,\delta_0,\lambda_0) = \sqrt{\left(\frac{\partial F}{\partial\beta}\delta\beta\right)^2 + \left(\frac{\partial F}{\partial\delta}\delta\delta\right)^2 + \left(\frac{\partial F}{\partial\lambda}\delta\lambda\right)^2}\Bigg|_{(m_{i,\min};\beta_0,\delta_0,\lambda_0)}. \tag{4.15}$$

The errors for the apparent magnitude minima which will be used as weights in the χ^2 minimization will therefore be calculated as

$$\delta m_{i,\min} = F(m_{i,\min};\beta_0,\delta_0,\lambda_0) + \delta F(m_{i,\min};\beta_0,\delta_0,\lambda_0) \tag{4.16}$$

for whichever distribution, Weibull or Fréchet, is determined to best fit the true quasar apparent magnitude distribution.

4.4 Calculation of Curve Fitting Formulae

The need for an efficient method of calculating luminosity distances from (3.16) for various values of $\mathbf{A}$ and z was mentioned in §4.3. The analysis for this project will be performed using *Maple 10* because of its invaluable nonlinear curve fitting routines. However, the cost of using these routines effectively is that they must be supplied with functions which are easily evaluated because *Maple*'s

numerical integration procedures tend to be extremely slow. For *Maple* to efficiently calculate the apparent magnitude values and their derivatives with respect to the parameters, which are essential for an accurate χ^2 minimization, we must therefore convert (3.16) to an easily solvable form containing elliptic functions.

We begin this discussion by rewriting the luminosity distance neglecting radiation density (3.16),

$$d_{L,s}(z) = \frac{c(1+z)}{H_0\sqrt{\Omega_M + \Omega_\Lambda - 1}} \sin\left(\int_1^{1+z} du \frac{\sqrt{\Omega_M + \Omega_\Lambda - 1}}{\sqrt{\Omega_M u^3 + (1 - \Omega_M - \Omega_\Lambda)u^2 + \Omega_\Lambda}}\right), \tag{4.17}$$

where the subscript s implies that the evaluation of (4.17) is only relatively straightforward for the spherical geometry, where $\Omega_M + \Omega_\Lambda > 1$. For calculational purposes it is therefore convenient to also write this equation for the two cases $\Omega_M + \Omega_\Lambda = 1$ and $\Omega_M + \Omega_\Lambda < 1$ – respectively, the flat and hyperbolic geometries – separately.

By noting $\sin \mathrm{i}u = \mathrm{i}\sinh u$, we find the luminosity distance in a hyperbolic universe,

$$d_{L,h}(z) = \frac{c(1+z)}{H_0\sqrt{1 - \Omega_M - \Omega_\Lambda}} \sinh\left(\int_1^{1+z} du \frac{\sqrt{1 - \Omega_M - \Omega_\Lambda}}{\sqrt{\Omega_M u^3 + (1 - \Omega_M - \Omega_\Lambda)u^2 + \Omega_\Lambda}}\right). \tag{4.18}$$

For the luminosity distance in a flat universe, we evaluate (4.17) in the limit as $\Omega_M + \Omega_\Lambda \to 1$, which yields the result,

$$d_{L,f}(z) = \frac{c(1+z)}{H_0} \int_1^{1+z} \frac{du}{\sqrt{\Omega_M u^3 + \Omega_\Lambda}}. \tag{4.19}$$

Thus, in the end (4.6) must be defined by the piecewise combination of (4.17) – (4.19):

$$m_i - M_{i,0} = \begin{cases} 5\log_{10}\left(\frac{d_{L,c}}{d_0}\right) - 2.5(1+\alpha+\beta)\log_{10}(1+z), & \text{if } k = -1, \\ 5\log_{10}\left(\frac{d_{L,f}}{d_0}\right) - 2.5(1+\alpha+\beta)\log_{10}(1+z), & \text{if } k = 0, \\ 5\log_{10}\left(\frac{d_{L,o}}{d_0}\right) - 2.5(1+\alpha+\beta)\log_{10}(1+z), & \text{if } k = 1. \end{cases} \tag{4.20}$$

All that remains is the determination of the elliptic function representations of (4.17) – (4.19). For the spherical and hyperbolic geometries, the elliptic integrals to be evaluated are the same. The evaluation of these integrals is fairly complicated and will be left for the moment. We will start with finding the elliptic function representation for the easier case; the flat geometry. By substituting $u = -(\Omega_\Lambda/\Omega_M)^{1/3}t$ in (4.19) we find

$$d_{L,f} = \frac{c(1+z)}{H_0} \frac{1}{\Omega_\Lambda^{1/6}\Omega_M^{1/3}} \int_{-\left(\frac{\Omega_M}{\Omega_\Lambda}\right)^{1/3}(1+z)}^{-\left(\frac{\Omega_M}{\Omega_\Lambda}\right)^{1/3}} \frac{dt}{\sqrt{1-t^3}}, \tag{4.21}$$

which may be evaluated using the results of Byrd and Friedman (1971); i.e. we have

$$\int_{-\infty}^{y} \frac{dt}{\sqrt{1-t^3}} = \frac{1}{3^{1/4}} F(\phi, k), \tag{4.22}$$

where $F(\phi, k)$ is the *normal elliptic integral of the first kind*, defined by

$$F(\phi, k) = \int_0^{\phi} \frac{d\theta}{\sqrt{1 - k^2\sin^2\theta}} \tag{4.23}$$

and the *argument* ϕ and *modulus* k for this specific integral are given by

$$\phi = \arccos\left(\frac{1-\sqrt{3}-y}{1+\sqrt{3}-y}\right) \tag{4.24}$$

and

$$k^2 = \frac{2+\sqrt{3}}{4} = \sin^2\left(\frac{5\pi}{12}\right), \tag{4.25}$$

which is valid when $y \leq 1$, i.e. as long as $\Omega_\Lambda \geq -\Omega_M$, which is implicit in this evaluation. Thus, we find the luminosity distance in flat spacetime,

$$\begin{aligned} d_{L,f} &= \frac{c(1+z)}{H_0}\frac{1}{\Omega_\Lambda^{1/6}\Omega_M^{1/3}}\left(\int_{-\infty}^{-\left(\frac{\Omega_M}{\Omega_\Lambda}\right)^{1/3}}\frac{dt}{\sqrt{1-t^3}} - \int_{-\infty}^{-\left(\frac{\Omega_M}{\Omega_\Lambda}\right)^{1/3}(1+z)}\frac{dt}{\sqrt{1-t^3}}\right) \\ &= \frac{c(1+z)}{H_0}\frac{1}{\Omega_\Lambda^{1/6}\Omega_M^{1/3}}\frac{1}{3^{1/4}}\left[F(\phi_{1,f},k) - F(\phi_{2,f},k)\right], \end{aligned} \tag{4.26}$$

where

$$\phi_{1,f} = \arccos\left(\frac{(1-\sqrt{3})\Omega_\Lambda^{1/3} + \Omega_M^{1/3}}{(1+\sqrt{3})\Omega_\Lambda^{1/3} + \Omega_M^{1/3}}\right), \tag{4.27}$$

$$\phi_{2,f} = \arccos\left(\frac{(1-\sqrt{3})\Omega_\Lambda^{1/3} + \Omega_M^{1/3}(1+z)}{(1+\sqrt{3})\Omega_\Lambda^{1/3} + \Omega_M^{1/3}(1+z)}\right), \tag{4.28}$$

and

$$k = \sin\left(\frac{5\pi}{12}\right). \tag{4.29}$$

The elliptic integral involved in the calculation of the luminosity distance for the curved geometries can be written as

$$\int_1^{1+z}\frac{du}{\sqrt{f(u)}}, \tag{4.30}$$

where

$$f(u) = u^3 + \frac{(1-\Omega_M-\Omega_\Lambda)}{\Omega_M}u^2 + \frac{\Omega_\Lambda}{\Omega_M}. \tag{4.31}$$

We would again like to evaluate this using a table of integrals. From Byrd and Friedman (1971) we have

$$\int_y^\infty \frac{du}{\sqrt{(u-a)[(u-b_1)^2+a_1^2]}} = \frac{1}{\sqrt{A}}F(\phi,k), \tag{4.32}$$

where if $a \leq y < \infty$, $a \,\epsilon\, \mathbb{R}$, and $b \,\epsilon\, \mathbb{C}$, so that $b_1 = \Re b = \frac{b+\bar{b}}{2}$, $a_1^2 = (\Im b)^2 = -\frac{(b-\bar{b})^2}{4}$, we have

$$A^2 \equiv (b_1-a)^2 + a_1^2, \tag{4.33}$$

$$k^2 = \frac{A+b_1-a}{2A}, \tag{4.34}$$

and

$$\phi = \arccos\left(\frac{y-a-A}{y-a+A}\right). \tag{4.35}$$

We will see shortly that $a < 0$ for all physical values of Ω_M and Ω_Λ so that we must have $a \leq y < \infty$ for finite values of z.

Rather than explicitly writing $f(u)$ in the form given in (4.32) we write it in a similar, but computationally more simplistic form,

$$f(u) = u^3 + \frac{(1-\Omega_M-\Omega_\Lambda)}{\Omega_M}u^2 + \frac{\Omega_\Lambda}{\Omega_M} = (u-a)(u^2+cu+ac), \tag{4.36}$$

so that we may obtain the parameters we need from

$$b_1 = -\frac{c}{2} \text{ and } a_1^2 = \frac{(4a-c)c}{4}, \tag{4.37}$$

and for completeness we may write

$$b_\pm = b_1 \pm \mathrm{i}a_1 = \frac{-c \pm \sqrt{c^2-4ac}}{2}. \tag{4.38}$$

Now, (4.36) is satisfied *iff*

$$a^3 + \frac{1-\Omega_M-\Omega_\Lambda}{\Omega_M}a^2 + \frac{\Omega_\Lambda}{\Omega_M} = 0. \tag{4.39}$$

To find the solution to this cubic, we substitute

$$x = a + \frac{1-\Omega_M-\Omega_\Lambda}{3\Omega_M} \tag{4.40}$$

to obtain

$$x^3 - \frac{(1-\Omega_M-\Omega_\Lambda)^2}{3\Omega_M^2}x + 2\frac{(1-\Omega_M-\Omega_\Lambda)^3}{27\Omega_M^3} + \frac{\Omega_\Lambda}{\Omega_M} = 0. \tag{4.41}$$

Now, we have transformed (4.39) to the form

$$x^3 = 3px + 2q, \tag{4.42}$$

for which the solution

$$x = (q-w)^{1/3} + (q+w)^{1/3} \equiv U + V, \tag{4.43}$$

where

$$w = (q^2-p^3)^{1/2}, \tag{4.44}$$

was first published by Gerolamo Cardano in 1545 (Penrose, 2005). There is only one real solution for $q^2 \geq p^3$. However, when $q^2 < p^3$ and w is imaginary there are three real solutions. The curve $q^2 = p^3$ has been plotted in the $\Omega_\Lambda - \Omega_M$ plane in Figure 4.7. The two regions where $q^2 < p^3$ are those labeled r2 and r5. Region r2 is particularly interesting because density parameters in this region lead to complex values of $\dot{a}$ in (2.42) for certain values of the scale factor; thus, density parameters in this region cannot be allowed because they contradict the assumption of the big bang. The curve between r5 and r1 is the border for which the universe would expand forever or collapse eventually and the curve between r3 and r4 is of little importance because $q^2 \geq p^3$ for $\Omega_\Lambda < 0$. Note that the curves $\Omega_\Lambda = 0$ and $\Omega_M = 0$ have been plotted in Figure 4.7 because of the implicit assumptions in (4.17) – (4.19) that these density parameters are nonzero.

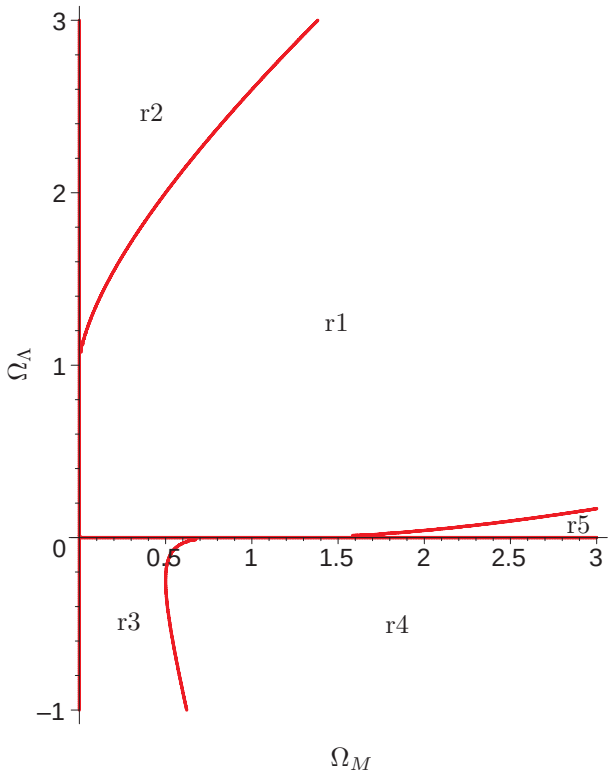

Figure 4.7: The curves $p = q$ in the $\Omega_\Lambda - \Omega_M$ plane, which display the valid density parameter ranges in big bang cosmology. $q^2 \geq p^3$ only in regions r1, r3, and r4. r1 is of particular importance because there can have been no big bang for parameter values here.

We find that x is purely real in region r1, which, according to the literature, should be our region of interest. Thus, the single solution to (4.41) in this region may be written:

$$U = -\left(\frac{\Omega_\Lambda}{2\Omega_M} + \frac{(1-\Omega_M-\Omega_\Lambda)^3}{27\Omega_M^3} - \frac{\Omega_\Lambda}{2\Omega_M}\sqrt{1 - \frac{4(1-\Omega_M-\Omega_\Lambda)^3}{27\Omega_\Lambda\Omega_M^2}}\right)^{1/3}, \tag{4.45}$$

$$V = -\left(\frac{\Omega_\Lambda}{2\Omega_M} + \frac{(1-\Omega_M-\Omega_\Lambda)^3}{27\Omega_M^3} + \frac{\Omega_\Lambda}{2\Omega_M}\sqrt{1 - \frac{4(1-\Omega_M-\Omega_\Lambda)^3}{27\Omega_\Lambda\Omega_M^2}}\right)^{1/3}, \tag{4.46}$$

from which we find the three parameters needed in solving (4.32):

$$a = U + V - \frac{1-\Omega_M-\Omega_\Lambda}{3\Omega_M}, \tag{4.47}$$

$$b_1 = U + V + \frac{2}{3}\frac{1-\Omega_M-\Omega_\Lambda}{\Omega_M}, \tag{4.48}$$

$$a_1^2 = 3(U+V)^2 - \frac{4}{3}\frac{(1-\Omega_M-\Omega_\Lambda)^2}{\Omega_M^2}. \tag{4.49}$$

With the constant a now defined, we are able to determine the density parameter values for which we may use (4.32) to evaluate (4.30). Figure 4.8 is a plot of the curves for which $a = 0$. In the central region of this figure, which covers a larger portion of the $\Omega_\Lambda - \Omega_M$ plane than region

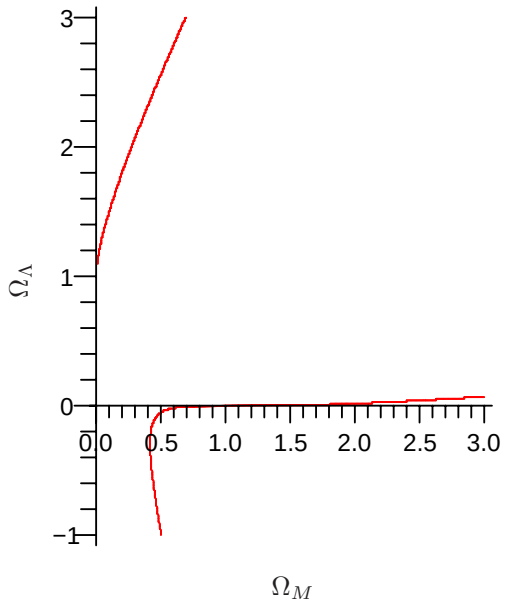

Figure 4.8: The curves $a = 0$ are used to illustrate the region in the $\Omega_\Lambda - \Omega_M$ plane for which $a < 0$ so that (4.33) – (4.35) may be used to determine (4.30). Region r1 from Figure 4.7 is a subset of the central region in this plot for which $a < 0$.

r1 in Figure 4.7, the values of a are negative. Therefore, the limits of integration in (4.30) will be greater than a for parameter values in r1, so we are justified in evaluating it using (4.33) – (4.35) and (4.45) – (4.49).

We may now write the equations for the luminosity distance in curved spacetime:

$$d_{L,s}(z) = \frac{c(1+z)}{H_0\sqrt{\Omega_M + \Omega_\Lambda - 1}} \sin\left(\sqrt{\frac{\Omega_M + \Omega_\Lambda - 1}{\Omega_M A}}\,[F(\phi_1, k) - F(\phi_2, k)]\right), \tag{4.50}$$

$$d_{L,h}(z) = \frac{c(1+z)}{H_0\sqrt{1 - \Omega_M - \Omega_\Lambda}} \sinh\left(\sqrt{\frac{1 - \Omega_M - \Omega_\Lambda}{\Omega_M A}}\,[F(\phi_1, k) - F(\phi_2, k)]\right), \tag{4.51}$$

where ϕ_1 and ϕ_2 are given by (4.35) with $y = 1$ and $y = 1 + z$, respectively.

Upon substitution of (4.26), (4.50), and (4.51) into the distance modulus equation (4.20), we find a degeneracy between the absolute magnitude M_i and Hubble's constant H_0. With the definition

$$B_s \equiv \frac{1}{\sqrt{\Omega_M + \Omega_\Lambda - 1}} \sin\left(\sqrt{\frac{\Omega_M + \Omega_\Lambda - 1}{\Omega_M A}}\,[F(\phi_1, k) - F(\phi_2, k)]\right), \tag{4.52}$$

this is illustrated in the spherical case as follows:

$$\begin{aligned} m_i &= M_{i,0} + 5\log_{10}\left(\frac{d_L}{d_0}\right) - 2.5(1+\alpha+\beta)\log_{10}(1+z) \\ &= M_{i,0} + 5\log_{10}\left(\frac{c}{H_0 d_0}\right) + 5\log_{10} B_s + 5\log_{10}(1+z) - 2.5(1+\alpha+\beta)\log_{10}(1+z) \end{aligned}$$

$$= M_{i,0} - 5\log_{10}\left(\frac{H_0 d_0}{c}\right) + 5\log_{10} B_s + 2.5(1-\alpha-\beta)\log_{10}(1+z). \tag{4.53}$$

For curvefitting purposes, we must therefore combine M_i and H_0 into one fit parameter,

$$A_1 \equiv M_{i,0} - 5\log_{10}\left(\frac{H_0 d_0}{c}\right). \tag{4.54}$$

The vector $\mathbf{A}$ from §4.3 is then defined as

$$\mathbf{A} \equiv [A_1, \Omega_M, \Omega_\Lambda, \alpha+\beta]. \tag{4.55}$$

By defining

$$B_h = \frac{1}{\sqrt{1-\Omega_M-\Omega_\Lambda}} \sin\left(\sqrt{\frac{1-\Omega_M-\Omega_\Lambda}{\Omega_M A}}\,[F(\phi_1,k) - F(\phi_2,k)]\right), \tag{4.56}$$

$$B_f = \frac{1}{\Omega_\Lambda^{1/6}\Omega_M^{1/3}} \frac{1}{3^{1/4}}\,[F(\phi_{1,f},k) - F(\phi_{2,f},k)], \tag{4.57}$$

we are now equipped with everything we need to write the piecewise apparent magnitude function

$$m_i(z;\mathbf{A}) = A_1 + 5\log_{10} B_{s,f,h}(A_2,A_3) + 2.5(1-A_4)\log_{10}(1+z), \tag{4.58}$$

where

$$B_{s,f,h}(A_2,A_3) \equiv \begin{cases} B_s(A_2,A_3), & \text{if } k=1, \\ B_f(A_2,A_3), & \text{if } k=0, \\ B_h(A_2,A_3), & \text{if } k=-1. \end{cases} \tag{4.59}$$

After formulating (4.58) in a step-by-step manner in *Maple* code, it is a simple matter to calculate its derivatives with respect to the parameters so that the curve fitting routines can efficiently determine the values of $\mathbf{A}$ for which the χ^2 variable (4.7) is at a minimum.

Chapter 5

Results

In Chapter 4, the stage was set for determining the values of the matter and vacuum cosmological density parameters, Ω_M and Ω_Λ, from a χ^2 minimization which uses a piecewise distance modulus equation for luminosity evolving quasars and apparent magnitudes of the brightest known quasars at varying redshifts with statistically determined errors. This analysis has been performed using nonlinear curvefitting routines within the Statistics and Optimization packages of *Maple 10*. In the following sections, the results of this analysis will be presented along with some specific procedural steps which were required.

5.1 Results from $m_{i,\mathbf{min}}$ Error Analysis

In §4.2 we found that the sample of apparent magnitude minima which is most representative of the luminosities of the brightest quasars at varying redshifts came from bins of width $\Delta z = 0.096$, beginning at $z = 2.6$. In §4.3, it was argued that the errors associated with the assumption that these minimal apparent magnitudes are the minimum possible apparent magnitudes, according to the distribution of all apparent magnitudes, could be calculated by fitting the minimal GEVD – more specifically, the Weibull and minimal Fréchet distributions – to all the apparent magnitudes in each bin.

Both the Weibull distribution

$$F_W(x;\beta,\lambda,\delta) = \begin{cases} 0, & \text{if } x < \lambda, \\ 1 - \exp\left[-\left(\frac{x-\lambda}{\delta}\right)^\beta\right], & \text{otherwise,} \end{cases} \tag{5.1}$$

and minimal Fréchet distribution,

$$F_F(x;\beta,\delta,\lambda) = \begin{cases} 1 - \exp\left[-\left(\frac{\delta}{\lambda-x}\right)^\beta\right], & \text{if } x \leq \lambda, \\ 1, & \text{otherwise,} \end{cases} \tag{5.2}$$

which have been rewritten here for convenience, were initially considered in separate maximum likelihood analyses. This was accomplished with the use of the *NLPSolve* routine in *Maple 10*'s Optimization package, which was able to maximize the log likelihood function (4.13) of the apparent magnitudes in each bin. Prior to calculating the log likelihood functions, both distributions were

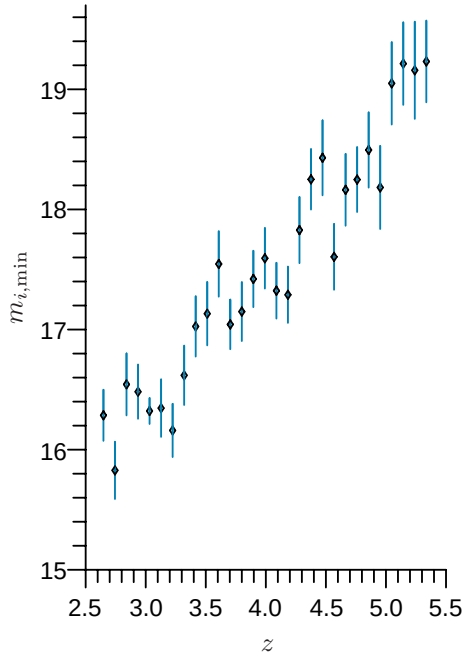

Figure 5.1: Quasar $m_{i,\min}$ error plot on the range $2.6 \leq z \leq 5.4$ from bins of width $\Delta z = 0.096$.

truncated by normalizing (5.1) and (5.2) so that $F_{W,F}(x;\beta,\lambda,\delta) = 1$ for $x \geq m_{i,\max}$, where $m_{i,\max} = 19.1$ or $m_{i,\max} = 20.2$, for $z < 3$ or $z > 3$, respectively.

It should also be noted here that the bin with endpoints on either side of $z = 3$ was fit only to the data on the side of $z = 3$ from which the minimal apparent magnitude came. However, the redshift bin midpoint was still used for χ^2 minimization. This choice was made so as to maintain that the actual redshifts of the apparent magnitude minima were drawn from a uniform distribution within their respective bins.

From the two separate analyses, it was determined that the maximum likelihood in all bins was greater for the Fréchet distribution. Because we have apparent magnitude measurements for only the brightest quasars, this analysis implies that the left tail of the quasar apparent magnitude distribution is *most likely* drawn from the minimal Fréchet distribution.

The errors for the minimal apparent magnitudes $\delta m_{i,\min}$ were subsequently calculated by adding the evaluation of (5.2) for the best fit parameters and minimal apparent magnitude $m_{i,\min}$ from each bin with the error in this calculation due to the uncertainty in the maximum likelihood analysis, which was determined from a Monte Carlo simulation. These data are displayed in Table 5.1 and Figure 5.1 for all redshift bins on $2.6 \leq z \leq 5.4$. Note that the furthest quasar in the Catalogue, with $z = 5.4135$ was not included in our final data set because it was the only quasar in its redshift bin; thus, no statistical analysis could be performed.

z	$m_{i,\min}$	$F_F(m_{i,\min})$	$\delta F_F(m_{i,\min})$	$\delta m_{i,\min}$
2.648	16.286	0.075	0.138	0.213
2.744	15.828	0.095	0.143	0.238
2.840	16.544	0.104	0.154	0.258
2.936	16.483	0.078	0.148	0.225
3.032	16.322	0.009	0.099	0.108
3.128	16.346	0.114	0.125	0.239
3.224	16.160	0.100	0.122	0.222
3.320	16.619	0.120	0.127	0.247
3.416	17.026	0.119	0.132	0.251
3.512	17.132	0.122	0.141	0.264
3.608	17.546	0.119	0.153	0.272
3.704	17.043	0.077	0.130	0.206
3.800	17.149	0.103	0.142	0.245
3.896	17.421	0.092	0.143	0.235
3.992	17.593	0.102	0.150	0.252
4.088	17.324	0.091	0.141	0.232
4.184	17.289	0.093	0.141	0.234
4.280	17.828	0.120	0.155	0.275
4.376	18.250	0.094	0.158	0.252
4.472	18.430	0.147	0.165	0.312
4.568	17.605	0.131	0.143	0.274
4.664	18.163	0.135	0.164	0.299
4.760	18.248	0.109	0.161	0.270
4.856	18.495	0.141	0.172	0.313
4.952	18.183	0.230	0.116	0.346
5.048	19.050	0.145	0.197	0.343
5.144	19.214	0.140	0.204	0.343
5.240	19.158	0.185	0.220	0.404
5.336	19.232	0.130	0.210	0.340

Table 5.1: Quasar $m_{i,\min}$ data on the range $2.6 \leq z \leq 5.4$ from bins of width $\Delta z = 0.096$. The z values used are the midpoints of the redshift bins. The total error in apparent magnitude $\delta m_{i,\min}$ comes from the addition of both $F_F(m_{i,\min})$ and $\delta F_F(m_{i,\min})$.

5.2 χ^2 Minimization Results and Uncertainties

In § 4.2, we used a qualitative argument to determine that the minimum redshift which may be modeled by our luminosity evolution equation is $z \approx 2.6$. However, the determination of the actual redshift range for which we may use our luminosity evolution model must come from a quantitative analysis. This has been done by comparing reduced χ^2 values, defined as χ^2 divided by degrees of freedom, χ^2/ν, for various redshift ranges within the data set listed in Table 5.1. The redshift range with the lowest reduced χ^2 value was then determined to be the optimal range.

According to the framework described in Chapter 4, the χ^2 minima for these various redshift ranges have been determined by finding the parameters

$$\mathbf{A} \equiv \left[M_i - 5\log_{10}\left(\frac{H_0 d_0}{c}\right), \Omega_M, \Omega_\Lambda, \alpha + \beta \right], \tag{5.3}$$

which minimize the χ^2 variable (4.7),

$$\chi^2(\mathbf{A}) = \sum_{j=1}^{N} \left[\frac{m_{i,\min,j} - m_i(z_j; \mathbf{A})}{\delta m_{i,\min,j}} \right]^2, \tag{5.4}$$

where the various data points $[z, m_{i,\min} \pm \delta m_{i,\min}]_j$ are listed in Table 5.1 and $m_i(z_j; \mathbf{A})$ is given by (4.58),

$$m_i(z; \mathbf{A}) = A_1 + 5\log_{10} B_{s,f,h}(A_2, A_3) + 2.5(1 - A_4)\log_{10}(1 + z). \tag{5.5}$$

This minimization was performed with *Maple 10*'s *LSSolve* routine, which is part of the Statistics package. A useful option in the *LSSolve* routine is that it admits nonlinear constraints on the parameters; thus, the problem was specified so that only physical values of the density parameters – i.e., values in the $\Omega_\Lambda - \Omega_M$ plane which do not fall in region r2 of Figure 4.7 – could be used.

After considering various endpoint values, the redshift range with the lowest reduced χ^2 value, $\chi^2/\nu = 1.23$, at the χ^2 minimum was determined to be $2.984 \leq z \leq 5.000$. The parameter values corresponding to this minimum are

$$\mathbf{A} = [7.39, 0.07, 1.13, -3.78]. \tag{5.6}$$

The distance modulus equation (5.5) with these parameter values has been plotted in Figure 5.2, along with the data in this range.

Confidence limits in the parameter values were estimated from the covariance matrix for this fit,

$$[C] = \begin{bmatrix} 1830 & -60.0 & -150 & 1650 \\ -60.0 & 2.12 & 5.07 & -54.9 \\ -150 & 5.07 & 12.5 & -136 \\ 1650 & -54.9 & -136 & 1490 \end{bmatrix}, \tag{5.7}$$

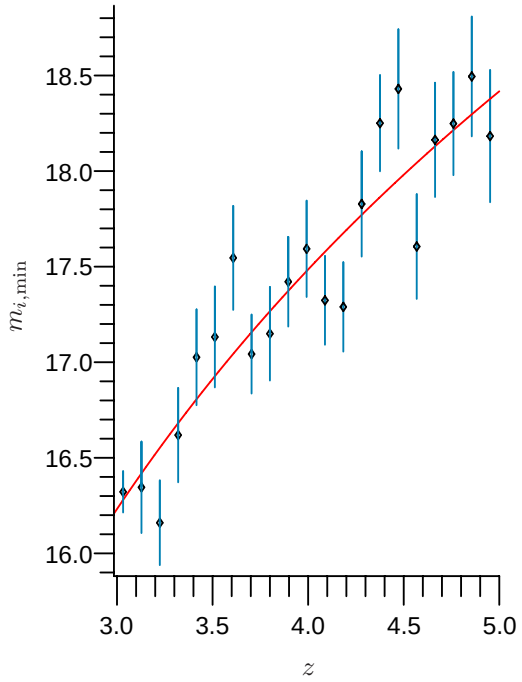

Figure 5.2: The brightest quasars on the interval $3 \leq z \leq 5$ and the apparent magnitude curve (5.5) with the parameter values resulting in the χ^2 minimum.

which was calculated by inverting the curvature matrix $[\alpha]$, defined by

$$\alpha_{kl} \equiv \frac{1}{2}\frac{\partial^2\chi^2}{\partial A_k \partial A_l} = \sum_{j=1}^{N} \frac{1}{\sigma_j^2}\left[\frac{\partial m_i(z_j;\mathbf{A})}{\partial A_k}\frac{\partial m_i(z_j;\mathbf{A})}{\partial A_l} - [m_{i,\,j} - m_i(z_j;\mathbf{A})]\frac{\partial^2 m_i(z_j;\mathbf{A})}{\partial A_k \partial A_l}\right] \tag{5.8}$$

(Press *et al.*, 1994). As long as the data are normally distributed about the actual physical curve – a point which will be addressed shortly – the square roots of the diagonal elements of $[C]$ are the uncertainties in the individual parameters. Therefore, the best fit parameter values with their uncertainties are

$$\mathbf{A} = [7.39 \pm 42.77, 0.07 \pm 1.46, 1.13 \pm 3.53, -3.78 \pm 38.56]. \tag{5.9}$$

In order to better understand these large uncertainties in Ω_M and Ω_Λ, a plot of the estimated 1-σ and 2-σ confidence regions in this plane has been constructed. This was done by plotting the ellipses defined by

$$\Delta\chi^2 = \begin{bmatrix} \Omega'_M & \Omega'_\Lambda \end{bmatrix} [C_{\mathrm{proj},M\Lambda}]^{-1} \begin{bmatrix} \Omega'_M \\ \Omega'_\Lambda \end{bmatrix}, \tag{5.10}$$

where the 1-σ and 2-σ quantiles are $\Delta\chi^2 = 2.30$ and 6.17 for a chi-squared distribution with two degrees of freedom and $[C_{\mathrm{proj},M\Lambda}]$ is the 2×2 intersection of the second and third rows and columns of $[C]$ (see Figure 5.3). This plot indicates that there is room within the uncertainties of this analysis for the literature values $\Omega_M \approx 0.3$ and $\Omega_\Lambda \approx 0.7$. However, the calculated ellipses

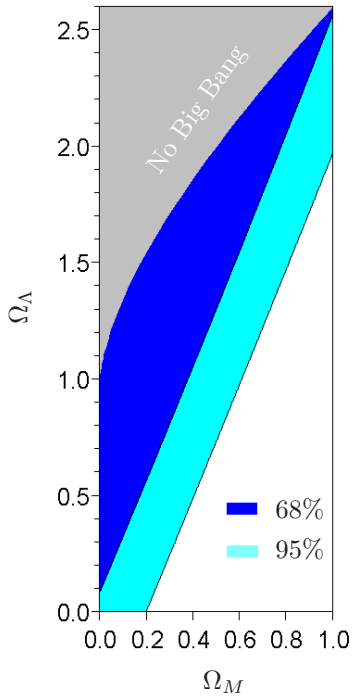

Figure 5.3: Confidence limits for the estimated model parameters in the $\Omega_M - \Omega_\Lambda$ plane. The boundaries of the ellipses which define these 1-σ and 2-σ confidence regions extend well into the non-physical regions – $\Omega_M < 0$ and $q^2 < p^3$ – of the Λ CDM model.

are quite large and the majority of the confidence region determined through this method falls outside the physical region, in the areas of the plane where there could have been no big bang, or where $\Omega_M < 0$. Therefore, another approach to this type of plot may provide a more accurate representation of the confidence limits.

It is becoming standard practice in this type of analysis to calculate confidence regions by plotting constant boundaries of a likelihood function, which in this analysis would come from the χ^2 variable. A discussion of this type of analysis, which uses Markov Chain Monte Carlos (MCMCs) to efficiently determine these boundaries by considering only parameter values near the desired confidence level, is given in Verde *et al.* (2003). However, it was decided that the MCMC approach was beyond the scope of the present analysis, which involves a nonstatistical data set and an elementary luminosity evolution equation. This brings us to the assumption that the data are normally distributed about the actual physical curve. This is a bold assumption to make and thus, the MCMC method, which would determine uncertainties based on the χ^2 landscape, is considered to be more accurate.

Chapter 6

Discussion

Although the final results of this analysis only agree loosely with the literature values, there are many possible (and exciting) explanations for the outcome presented in the previous chapter. Therefore, although this analysis is only in agreement with the literature values for Ω_M and Ω_Λ at the 95% confidence level, this project was successful for a couple of reasons:

i. The main goal for this project was to construct a method for using the large catalogue of SDSS quasars to determine values for Ω_M and Ω_Λ, which has been accomplished. There were many points in the analysis where assumptions had to be made; any of which could have led to errors in the results. Therefore, this study presents many possibilities for future work.

ii. A new method for statistically analyzing apparent magnitudes of the brightest quasars, or any extreme values of a distribution for that matter, has been developed during this project. This method has the possibility of seeing many applications and is perhaps the greatest success of this thesis because it allowed for a statistical determination of cosmological parameters from data located at a distance for which these values have not previously been determined.

The second point here has to do with the error bars calculated for the apparent magnitude minima. Unfortunately, the success of this purely statistical method may not be determined conclusively, and may only be tested through repetition. With that said, the logic behind this approach – that the probability of the existence of brighter quasars is a measure of the error in the value of the observed extreme value – does make intuitive sense. In any case, this method is not likely a large contributor to the error in this analysis because of the low degree to which the errors influence the parameter values of the χ^2 minimum. In fact, the most erroneous factor in this error analysis was most likely that in the end there was no choice but to use a nonstatistical sample of quasars. As mentioned in §4.3, this may be rectified upon release of a paper, which is to be written by the SDSS collaboration, detailing the construction of a statistical sample from the quasar catalogue.

The most likely explanation for the discrepancy in the final results is that the analysis did not exhaust all possible options. There were some significant assumptions made in the development of this project, each of which presents some possibility for future work.

First of all, the form of luminosity evolution of high redshift quasars was assumed to be well approximated by a power law,

$$L(z) = L_0(1+z)^{\beta}. \tag{6.1}$$

It was argued that this function is capable of closely fitting the shape of the actual luminosity evolution of quasars in some region, and therefore, if another luminosity evolution equation were to be used instead, the frequency continuum index, α, could not be set as a free parameter due to its degeneracy with β. However, α has been measured using independent methods (Vanden Berk *et al.*, 2001), and therefore its best estimated value could be used so that a more theoretical luminosity evolution function could be modeled. For instance, the luminosity of the brightest quasars could be determined by considering the Eddington limit of the maximum supermassive black hole mass at varying redshifts.

One point to mention here is that the covariance matrix (5.7) presented in §5.2 displays little covariance between either Ω_M or Ω_Λ and the $\alpha + \beta$ term. Therefore, this luminosity evolution equation should not have had a large influence on the final values of the density parameters, with the exception of a couple of possibilities: it may have affected the final results if either its shape was not general enough to account for the actual luminosity evolution, or if it introduced a preference to a specific redshift range for which the data were not normally distributed about the actual physical curve (which would have been significant only if the error bars did not properly account for this effect).

The luminosity evolution equation is, however, not the only possible source of error in this analysis. As mentioned earlier, this project has used a data set located in a distance range which has never before been used directly in the determination of cosmological parameters. Therefore, previous analyses have not been complete and the values of cosmological parameters which they have derived may be subject to observational bias. As such, certain assumptions of the Λ CDM model should also be investigated.

For instance, we assumed a vacuum equation of state $p_\Lambda = w\rho_\Lambda$ with $w = -1$ for constant Λ. However, any time-dependent function, $\Lambda(a)$, satisfying conservation of energy and momentum is admitted by the Einstein equation. Therefore, values other than $w = -1$ should be considered for completeness. Leaving w as a free parameter leads to a scale factor dependent energy density for the vacuum,

$$\rho_\Lambda = \rho_{\Lambda,0}\left(\frac{a_0}{a}\right)^{3(1+w)}, \tag{6.2}$$

which modifies the rate of change of the scale factor to

$$\dot{a} = a_0 H_0 \sqrt{\Omega_M\left(\frac{a_0}{a} - 1\right) + \Omega_R\left(\frac{a_0^2}{a^2} - 1\right) + \Omega_\Lambda\left(\frac{a_0^{1+3w}}{a^{1+3w}} - 1\right) + 1}. \tag{6.3}$$

Therefore, a future analysis could be performed in which w was treated as a free parameter for χ^2 minimization.

Another assumption that was made was that the neutrino energy density, with $\Omega_\nu < 0.01$, is negligible compared to Ω_M and Ω_Λ. However, if $T_\nu \gg \frac{m_\nu c^2}{k_B}$, so that $p_\nu = 1/3\rho_\nu$ and neutrinos contribute to Ω_R, the radiation energy density may not be negligible compared with the matter and vacuum energy densities if $\Omega_\nu \sim 10^{-2}$. This is especially true at high redshifts, because (6.3) and (2.7) imply that we are actually comparing $\Omega_R(1+z)^2$ with $\Omega_M(1+z)$ and $\Omega_\Lambda(1+z)^{1+3w}$. Therefore, it may not only be required that Ω_R is included in this analysis, but this method may actually be capable of determining bounds for Ω_R. Then, because Ω_γ has been well determined from CMB measurements, we would have upper and lower bounds for Ω_ν, and therefore $\sum m_\nu$, which would be a significant result for particle physics.

Chapter 7

Conclusion

In this thesis, a new method has been developed for determining values of the cosmological density parameters, Ω_M and Ω_Λ, using a catalogue of quasars from the Sloan Digital Sky Survey. This was accomplished by selecting the brightest quasars within redshift bins and performing a χ^2 minimization involving the i band apparent magnitudes of these quasars and a luminosity evolving distance modulus equation (4.58) to determine the optimal values for the parameters of the luminosity distance, Ω_M and Ω_Λ. The errors used in this analysis were evaluated by fitting the generalized extreme value distribution to the apparent magnitude distribution in each bin. The bright tail of the quasar apparent magnitude distribution was found to be most likely drawn from the Fréchet distribution (4.11); therefore, the evaluation of the CDF of the best fit Fréchet distribution to the apparent magnitudes of the quasars in each bin was evaluated at the minimum apparent magnitude. This value, which is interpreted as the probability of the existence of a brighter quasar, was used as the uncertainty in the χ^2 minimization.

The redshift range for which the luminosity evolution equation (4.3) was determined to best fit the brightest apparent magnitude values was $3 \leq z \leq 5$. The values of the density parameters which minimize χ^2 in this range are $\Omega_M = 0.07 \pm 1.46$ and $\Omega_\Lambda = 1.13 \pm 3.53$. These values have large uncertainties, which could be the result of either the method in which they were determined (the covariance matrix approach) or a problem in the theory. The fact that they are so different from the literature values, $\Omega_M \approx 0.3$ and $\Omega_\Lambda \approx 0.7$, suggests the latter to be more likely. Therefore, possible sources of error in the theory, such as an incorrect form of luminosity evolution, neglecting radiation density for this high redshift analysis, and the assumption of an equation of state for dark energy with $w = -1$ have been discussed in Chapter 6.

This project has led quite naturally to questions about the cosmological theory for the early stages of the universe and future work will therefore be designed to address these questions. However, the main goal of this project, which was to take a large catalogue of quasars and develop a method for determining values of the cosmological density parameters from these extremely distant objects, has been accomplished.

References

Alpher, R. A., and R. Herman, 1948, Nature **74**, 774.

Astier, P., J. Guy, N. Regnault, R. Pain, E. Aubourg, D. Balam, S. Basa, R. G. Carlberg, S. Fabbro, D. Fouchez, I. M. Hook, D. A. Howell, *et al.*, 2006, Astronomy & Astrophysics **447**, 31.

Byrd, P. F., and M. D. Friedman, 1971, *Handbook of Elliptic Integrals for Engineers and Scientists* (Springer-Verlag, New York), 2nd edition.

Carroll, B. W., and D. A. Ostlie, 2007, *An Introduction to Modern Astrophysics* (Pearson Education, Inc., publishing as Addison Wesley, San Fransisco), 2nd edition.

Castillo, E., A. S. Hadi, N. Balakrishnan, and J. M. Sarabia, 2005, *Extreme Value and Related Models with Applications in Engineering and Science* (John Wiley & Sons, Inc., United States of America).

Cole, S., W. J. Percival, J. A. Peacock, P. Norberg, C. M. Baugh, C. S. Frenk, I. Baldry, J. Bland-Hawthorn, T. Bridges, R. Cannon, M. Colless, C. Collins, *et al.*, 2005, The Monthly Notices of the Royal Astronomical Society **362**, 505.

Colless, M., G. Dalton, S. Maddox, W. Sutherland, P. Norberg, S. Cole, J. Bland-Hawthorn, T. Bridges, R. Cannon, C. Collins, W. Couch, N. Cross, *et al.*, 2001, The Monthly Notices of the Royal Astronomical Society **328**, 1039.

de Sitter, W., 1917, The Monthly Notices of the Royal Astronomical Society **78**, 3.

Einstein, A., 1915a, Sitzungsberichte der Königlich Preußischen Akademie der Wissenschaften (Berlin) , 844.

Einstein, A., 1915b, Sitzungsberichte der Königlich Preußischen Akademie der Wissenschaften (Berlin) , 778.

Einstein, A., 1915c, Sitzungsberichte der Königlich Preußischen Akademie der Wissenschaften (Berlin) , 799.

Foley, R. J., A. V. Filippenko, C. Aguilera, A. C. Becker, S. Blondin, P. Challis, A. Clocchiatti, R. Covarrubias, T. M. Davis, P. M. Garnavich, S. Jha, R. P. Kirshner, *et al.*, 2007, ArXiv e-prints `0710.2338`.

Gamow, G., 1948, Nature **162**, 680.

Greenstein, J. L., and T. A. Matthews, 1963, The Astronomical Journal **68**, 279.

Hartle, J. B., 2003, *Gravity: An Introduction to Einstein's General Relativity* (Pearson Education, Inc., publishing as Addison Wesley, San Fransisco).

Hubble, E. P., 1926, The Astrophysical Journal **63**, 236.

Hubble, E. P., 1929, Proceedings of the National Academy of Science **15**, 168.

Jackson, J. C., and M. Dodgson, 2002, The Monthly Notices of the Royal Astronomical Society **332**, 479.

Knop, R. A., G. Aldering, R. Amanullah, P. Astier, G. Blanc, M. S. Burns, A. Conley, S. E. Deustua, M. Doi, R. Ellis, S. Fabbro, G. Folatelli, *et al.*, 2003, The Astrophysical Journal **598**, 102.

Maddox, S. J., G. Efstathiou, and W. J. Sutherland, 1990, The Monthly Notices of the Royal Astronomical Society **246**, 433.

Mather, J. C., D. J. Fixsen, R. A. Shafer, C. Mosier, and D. T. Wilkinson, 1999, The Astrophysical Journal **512**, 511.

Matthews, T. A., and A. R. Sandage, 1963, The Astrophysical Journal **138**, 30.

Peebles, P. J. E., 1993, *Principles of Physical Cosmology* (Princeton University Press, Princeton, New Jersey).

Penrose, R., 2005, *The Road to Reality: A Complete Guide to the Laws of the Universe* (Vintage Books, London).

Penzias, A. A., and R. W. Wilson, 1965, The Astrophysical Journal **142**, 419.

Press, W. H., S. A. Teukolsky, W. T. Vetterling, and B. P. Flannery, 1994, *Numerical Recipes in C: The Art of Scientific Computing* (Cambridge University Press, New York), 2nd edition.

Riess, A. G., L.-G. Strolger, S. Casertano, H. C. Ferguson, B. Mobasher, B. Gold, P. J. Challis, A. V. Filippenko, S. Jha, W. Li, J. Tonry, R. Foley, *et al.*, 2007, The Astrophysical Journal **659**, 98.

Robertson, H. P., 1935, The Astrophysical Journal **82**, 284.

Schlegel, D. J., D. P. Finkbeiner, and M. Davis, 1998, The Astrophysical Journal **500**, 525.

Schneider, D. P., J. E. Gunn, and J. G. Hoessel, 1983, The Astrophysical Journal **264**, 337.

Schneider, D. P., P. B. Hall, G. T. Richards, M. A. Strauss, D. E. Vanden Berk, S. F. Anderson, W. N. Brandt, X. Fan, S. Jester, J. Gray, J. E. Gunn, M. U. SubbaRao, *et al.*, 2007, The Astronomical Journal **134**, 102.

Schneider, D. P., G. T. Richards, X. Fan, P. B. Hall, M. A. Strauss, D. E. Vanden Berk, J. E. Gunn, H. J. Newberg, T. A. Reichard, C. Stoughton, W. Voges, B. Yanny, *et al.*, 2002, The Astronomical Journal **123**, 567.

Spergel, D. N., R. Bean, O. Doré, M. R. Nolta, C. L. Bennett, J. Dunkley, G. Hinshaw, N. Jarosik, E. Komatsu, L. Page, H. V. Peiris, L. Verde, *et al.*, 2007, The Astrophysical Journal Suppliment Series **170**, 377.

Spergel, D. N., L. Verde, H. V. Peiris, E. Komatsu, M. R. Nolta, C. L. Bennett, M. Halpern, G. Hinshaw, N. Jarosik, A. Kogut, M. Limon, S. S. Meyer, *et al.*, 2003, The Astrophysical Journal Suppliment Series **148**, 175.

Tonry, J. L., B. P. Schmidt, B. Barris, P. Candia, P. Challis, A. Clocchiatti, A. L. Coil, A. V. Filippenko, P. Garnavich, C. Hogan, S. T. Holland, S. Jha, *et al.*, 2003, The Astrophysical Journal **594**, 1.

Vanden Berk, D. E., G. T. Richards, A. Bauer, M. A. Strauss, D. P. Schneider, T. M. Heckman, D. G. York, P. B. Hall, X. Fan, G. R. Knapp, S. F. Anderson, J. Annis, *et al.*, 2001, The Astronomical Journal **122**, 549.

Verde, L., H. V. Peiris, D. N. Spergel, M. R. Nolta, C. L. Bennett, M. Halpern, G. Hinshaw, N. Jarosik, A. Kogut, M. Limon, S. S. Meyer, L. Page, *et al.*, 2003, The Astrophysical Journal Suppliment Series **148**, 195.

Walker, A. G., 1935, The Monthly Notices of the Royal Astronomical Society **95**, 263.

Yao, W.-M., C. Amsler, D. Asner, R. Barnett, J. Beringer, P. Burchat, C. Carone, C. Caso, O. Dahl, G. D'Ambrosio, A. DeGouvea, M. Doser, *et al.*, 2006, Journal of Physics G **33**, 1+, URL `http://pdg.lbl.gov`.

York, D. G., J. Adelman, J. E. Anderson, Jr., S. F. Anderson, J. Annis, N. A. Bahcall, J. A. Bakken, R. Barkhouser, S. Bastian, E. Berman, W. N. Boroski, S. Bracker, *et al.*, 2000, The Astronomical Journal **120**, 1579.